Modeling dry friction in DIANA

van de Vrande, B.L.

Award date:
1996

Modeling Dry Friction in DIANA

Bram L. van de Vrande

WFW rapport nr. 96.084

Afstudeerverslag

Hoogleraar: Prof. dr. ir. D. H. van Campen
Begeleider: Dr. ir. A. de Kraker

Technische Universiteit Eindhoven
Faculteit Werktuigbouwkunde
Vakgroep Fundamentele Werktuigkunde (WFW)

Juni 1996

Contents

Samenvatting

Droge wrijving is het verschijnsel, waarbij twee lichamen, die met elkaar in contact zijn, weerstand bieden tegen een relatieve beweging. In de praktijk veroorzaakt droge wrijving vaak ongewenste bijverschijnselen. Het kan namelijk zichzelf in stand houdende oscillaties opwekken, die stick—slip trillingen worden genoemd.

In boorstangen treden stick—slip torsie-trillingen op. Boorstangen worden gebruikt bij het produceren van olie en gas. Hierbij worden putten geboord met een draaiende beitel. De beitel wordt aangedreven door een elektrische motor aan het oppervlak, die zijn torsie doorgeeft via de boorstang. Tussen de beitel en delen van de boorstang aan de ene kant, en het gesteente aan de andere kant, treedt droge wrijving op. Als een boorstang een stick—slip torsie-trilling uitvoert, draait het bovenste gedeelte van de boorstang met een constante snelheid rond, terwijl de snelheid van de beitel varieert tussen nul (de stick fase) en een snelheid, die veel hoger ligt dan die van het bovenste gedeelte (de slip fase). Dit kan beschadingen met zich meebrengen.

In de literatuur wordt droge wrijving op verschillende manieren gemodelleerd. De wrijvingswet van Coulomb is het bekendste. Ten gevolge van het discontinue karakter van droge wrijving, ontstaan er zwaar niet-lineaire differentiaalvergelijkingen. In dit rapport worden periodieke oplossingen bepaald van 1– en 2–DOF systemen, die droge wrijving ondervinden, met behulp van module STRDYN, behorende bij het eindige elementen pakket DIANA. Deze module biedt een aantal numerieke algoritmes om eindige elementenmodellen met lokale niet-lineariteiten te bestuderen. Om numerieke problemen te voorkomen, dienen gladde benaderingen van de discontinue wrijvingsmodellen te worden gebruikt.

Als eerste zijn 1– en 2–DOF modellen, overgenomen uit de literatuur, in DIANA gemodelleerd. Het wrijvingsmodel is benaderd met een arctan–functie. Met behulp van een semi-analytische oplossing van het 1–DOF model, zijn relatieve fouten in de DIANA oplossingen bepaald. Een goede overeenkomst is gevonden tussen de resultaten van DIANA en die uit de literatuur. Hierna is een 1 graad van vrijheid boorstangmodel met Coulombse

wrijving in DIANA gemodelleerd, waarbij gebruik is gemaakt van een vierde graads polynoom voor de benadering van het wrijvingsmodel. Ook hier in een semi-analytische oplossing gebruikt om relatieve fouten te bepalen. Opnieuw is een goede overeenkomst gevonden tussen de resultaten.

Summary

Dry friction is the phenomenon, in which to bodies, that are in contact with each other, offer resistance to a relative motion. In engineering practice, dry friction often causes undesirable side effects. It can namely induce self-sustained oscillations, called stick—slip vibrations.

Torsional stick—slip vibrations are observed in drill strings, that are used in rotary drilling for oil and gas. In rotary drilling, deep wells are drilled with a rock-crushing tool, called a drill bit. The drill bit is driven by an electric motor at the surface, whose torque is transmitted by the drill string. Between the drill bit and parts of the drill string on the one hand, and the rock on the other hand, dry friction occurs. When a drill string is undergoing a torsional stick—slip vibration, the top is rotating at a constant speed, whereas the speed at the drill bit varies between zero (the stick phase) and a speed, much higher than the speed at the top (the slip phase), which can lead to damage of drilling components.

In literature, different dry friction models can be found, of which Coulomb's friction law is the most familiar. Because of the discontinuous nature of dry friction, highly nonlinear differential equations are found. In this report, periodic solutions of 1– and 2–DOF systems, experiencing dry friction are determined, using module STRDYN of the finite element code DIANA. This module offers several numerical algorithms for investigating finite element models with local nonlinearities. To avoid numerical complications, smooth approximations of the discontinuous friction model must be used.

First, 1– and 2–DOF dry friction models, taken from literature, are modeled in DIANA. The friction model is approximated, using an arctan–function. A semi-analytic solution to the 1–DOF model is used, to determine relative errors in the DIANA solutions. Good correspondence is found between the DIANA results and the results from literature. Next, a 1–DOF drill string model with friction, according to Coulomb's law, is modeled in DIANA, using a 4th-order polynomial to approximate the friction model. Here, also a semi-analytic solution is used, to determine relative errors. Again, good correspondence is found between the results.

Chapter 1

Introduction

In this introduction, dry friction is explained and the motivation and the objective of this report are elucidated.

1.1 Dry friction

Dry friction is the natural phenomenon, in which two bodies (in Fig. 1.1 represented by 1 and 2), that are in contact with each other, offer resistance to a relative motion. On each of the two bodies, a *dynamic* friction force $\vec{F}$ appears, that acts in the opposite direction of the relative velocity $\vec{v}_{\text{rel}} \neq \vec{0}$. This velocity is defined as the velocity of the considered body, relative to the other body. If there is no relative motion ($\vec{v}_{\text{rel}} = \vec{0}$), a *static* friction force $\vec{F}$ can appear, that is opposite to the direction of the projection onto the contact plane of the applied force $\vec{F}_{\text{A}}$. The contact plane is defined at the contact between the bodies and is perpendicular to the normal force $\vec{F}_{\text{N}}$. Fig. 1.1 shows the forces, acting on body 1, for the cases, that (a), there

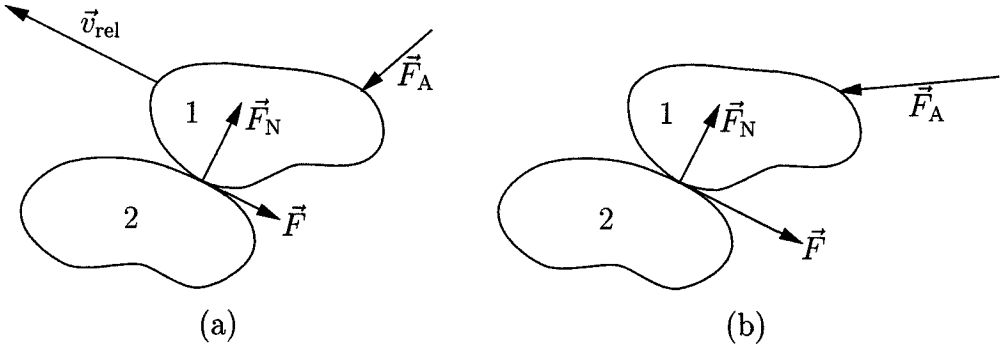

Figure 1.1: Dry friction, (a) *slip*, (b) *stick*

is relative motion with a *dynamic* friction force $\vec{F}$ (the *slip* phase) and (b), there is no relative motion with a *static* friction force $\vec{F}$ (the *stick* phase).

The magnitude of the dynamic friction force is modeled as a linear function of the magnitude of the normal force. That is, $F = \mu F_N$ (if $\vec{v}_{rel} \neq \vec{0}$), where $F \equiv \|\vec{F}\|$ and $F_N \equiv \|\vec{F}_N\|$. Parameter $\mu = \mu(v_{rel})$ is the dynamic friction coefficient, that is a function of the magnitude of the relative velocity, where $v_{rel} \equiv \|\vec{v}_{rel}\|$. The static friction force is a constraining force, whose magnitude equals the magnitude of the projection onto the contact plane of the applied force, but does not exceed a maximum static friction force $F_s \equiv \mu_0 F_N$. That is, $F \leq \mu_0 F_N$ (if $\vec{v}_{rel} = \vec{0}$), where μ_0 is the static friction coefficient. When there is no relative motion and the applied force overcomes the maximum static friction force, a relative motion is initiated.

In literature, the dependence of the dynamic friction coefficient on the magnitude of the relative velocity has been modeled in several, different ways. In Coulomb's friction law, μ is assumed to be constant, where $\mu \leq \mu_0$. In most other models, the dynamic friction coefficient is modeled as a decreasing function of the magnitude of the relative velocity. This decrease in μ for increasing v_{rel} has also been observed in experiments (see for instance Popp and Stelter [11]).

In engineering practice, dry friction often causes undesirable side effects. It can namely induce self-sustained oscillations, called stick—slip vibrations, that can shorten the lifespan of mechanical parts. Examples of these vibrations are grating brakes and chattering machine tools. Some stick—slip vibrations, that happen in everyday life, are squeaking chalks and creaking doors.

1.2 Motivation

The motivation for this report is the torsional stick—slip vibration, observed in drill strings at the Shell oil company. Drill strings are used in rotary drilling, which is the most common method for the exploration and production of oil and gas.

In rotary drilling, deep wells are drilled with a rock-crushing tool, called a drill bit. The drill bit is driven by an electric motor at the surface, whose torque is transmitted by a drill string. This drill string consists mainly of slender, steel tubes, called drill pipes, that are coupled with threaded connections and have a diameter, that is smaller than that of the bore hole. At the lower part, drill collars and stabilizers are used, to avoid buckling of the drill string. These drill collars are thick walled pipes and stabilizers are cylindrical elements, that fit loosely in the bore hole. At the top, the drill

string is supported by a drilling rig.

During the drilling process, the length of the drill string can become several kilometers. With an average diameter of about one decimeter, its ratio between length and diameter can be larger than that of a human hair.

Between the drill bit, the drill collars and the stabilizers on the one hand, and the rock on the other hand, dry friction occurs, which is responsible for the observed stick—slip vibration. When the drill string is undergoing this vibration, the rotation speed at the top of the drill string is approximately constant, whereas the speed at the bit varies between zero (the stick phase) and a speed, much higher than the speed at the top (during the slip phase). Because the stick—slip vibration can result in failure of drilling components, at KSEPL[1] research is done, to develop methods, that can prevent it.

1.3 Objective

Because of the discontinuous nature of dry friction, highly nonlinear differential equations are found, when dynamic systems, experiencing dry friction, are modeled. The objective of this report is to find periodic solutions of such models, using a dedicated module in the finite element code DIANA [3]. This module is called STRDYN ('structural dynamics') and comprises several numerical algorithms for investigating finite element models with local nonlinearities.

Here, the shooting method is used, to determine periodic solutions, together with a path following algorithm, to calculate branches of periodic solutions, if a design variable of the system is varied.

In chapter 2 these numerical algorithms are treated briefly. Chapter 3 discusses some example systems, that are modeled in DIANA. A drill string model is presented in chapter 4 and, finally in chapter 5, some conclusions are summarized.

[1] KSEPL (Koninklijke/Shell Exploratie en Produktie Laboratorium) is the oil and gas exploration and production laboratory of Shell Research in Rijswijk, The Netherlands.

Chapter 2

Numerical algorithms

In this chapter, a representation of dynamic systems is defined and some of the numerical algorithms from module STRDYN, that are used in this report, are treated briefly.

2.1 Dynamic systems

An nth-order, autonomous, nonlinear dynamic system is represented by the state equation

$$\dot{\underset{\sim}{x}} = \underset{\sim}{f}(\underset{\sim}{x}), \tag{2.1}$$

where $\dot{\underset{\sim}{x}} \equiv \mathrm{d}\underset{\sim}{x}/\mathrm{d}t$, $\underset{\sim}{x}$ is a column with the n state variables of the system, t is time and $\underset{\sim}{f}$ is a column of nonlinear functions of the components of $\underset{\sim}{x}$. Since $\underset{\sim}{f}$ does not depend on t, the system is called autonomous, as opposed to non-autonomous systems, where $\underset{\sim}{f}$ is a function of both $\underset{\sim}{x}$ and t. In this report, only autonomous systems are dealt with.

In an initial value problem, the initial condition is usually given at $t = t_0$. Because $\underset{\sim}{f}$ is independent on t, solutions based at time $t_0 \neq 0$, can always be translated to $t_0 = 0$. Hence, the initial condition reads

$$\underset{\sim}{x}(t = 0) = \underset{\sim}{x}_0. \tag{2.2}$$

The solution to (2.1) is often written as $\underset{\sim}{\phi}_t(\underset{\sim}{x}_0)$, to explicitly show the dependence on the initial condition in (2.2).

2.2 Shooting method

To find periodic solutions, one could integrate (2.1), until a steady state is reached. An advantage of this approach is the fact, that there is always

convergence. Moreover, both quasi-periodic and chaotic attractors can be found, as well. Disadvantages are, that it can be very time consuming and unstable solutions will not be found.

A more sensible procedure is to solve a 2–point boundary value problem, like the autonomous shooting method (taken from Parker and Chua [10]), in which solutions are sought of

$$\underset{\sim}{H}(\underset{\sim}{x}, T) \equiv \underset{\sim}{\phi}_T(\underset{\sim}{x}) - \underset{\sim}{x} = \underset{\sim}{0}, \tag{2.3}$$

where T is the period time of the periodic solution. Since (2.3) is a system of n equations in $n+1$ unknowns (the n components of $\underset{\sim}{x}$ and period T), it cannot be solved directly. Instead, $\underset{\sim}{y} \equiv \underset{\sim}{H}(\underset{\sim}{x}, T)$ is linearized, to obtain

$$\Delta\underset{\sim}{y} \approx \frac{\partial \underset{\sim}{H}}{\partial \underset{\sim}{x}}\Delta\underset{\sim}{x} + \frac{\partial \underset{\sim}{H}}{\partial T}\Delta T = (\underline{\Phi}_T(\underset{\sim}{x}) - \underline{I})\Delta\underset{\sim}{x} + \underset{\sim}{f}(\underset{\sim}{\phi}_T(\underset{\sim}{x}))\Delta T, \tag{2.4}$$

where matrix $\underline{\Phi}_T(\underset{\sim}{x})$ results from the variational equation (see appendix A). To achieve $\underset{\sim}{H} \approx \underset{\sim}{0}$, $\Delta\underset{\sim}{x}$ and ΔT will be chosen such, that $\Delta\underset{\sim}{y} = -\underset{\sim}{H}$. This value of $\Delta\underset{\sim}{y}$ is substituted in (2.4), giving

$$-\underset{\sim}{H} = (\underline{\Phi}_T(\underset{\sim}{x}) - \underline{I})\Delta\underset{\sim}{x} + \underset{\sim}{f}(\underset{\sim}{\phi}_T(\underset{\sim}{x}))\Delta T. \tag{2.5}$$

To make this system solvable, a constraint is added, which restricts the state correction term $\Delta\underset{\sim}{x}$ to be orthogonal to $\underset{\sim}{f}$, given by

$$\underset{\sim}{f}(\underset{\sim}{x})^{\mathrm{T}}\Delta\underset{\sim}{x} = 0. \tag{2.6}$$

From (2.5) and (2.6), the following iterative scheme is assembled, with which zeros of $\underset{\sim}{H}$ can be found, using initial guesses $\underset{\sim}{x}^{(0)}$ and $T^{(0)}$.

$$\begin{bmatrix} \underline{\Phi}_{T^{(i)}}(\underset{\sim}{x}^{(i)}) - \underline{I} & \underset{\sim}{f}(\underset{\sim}{\phi}_{T^{(i)}}(\underset{\sim}{x}^{(i)})) \\ \underset{\sim}{f}(\underset{\sim}{x}^{(i)})^{\mathrm{T}} & 0 \end{bmatrix} \begin{bmatrix} \Delta\underset{\sim}{x}^{(i)} \\ \Delta T^{(i)} \end{bmatrix} = \begin{bmatrix} \underset{\sim}{x}^{(i)} - \underset{\sim}{\phi}_{T^{(i)}}(\underset{\sim}{x}^{(i)}) \\ 0 \end{bmatrix} \tag{2.7}$$

$$\begin{bmatrix} \underset{\sim}{x}^{(i+1)} \\ T^{(i+1)} \end{bmatrix} = \begin{bmatrix} \underset{\sim}{x}^{(i)} \\ T^{(i)} \end{bmatrix} + \begin{bmatrix} \Delta\underset{\sim}{x}^{(i)} \\ \Delta T^{(i)} \end{bmatrix} \tag{2.8}$$

The superscripts have been added to indicate the iteration count. This scheme is reiterated, until some convergence criterion is met. There is a clear similarity to the Newton–Raphson algorithm, so the same convergence properties apply. When the shooting method returns values $\hat{\underset{\sim}{x}}$ and $\hat{T}$, it should be tested, whether $\hat{T}$ is the minimum period of the solution, since it could be a multiple of the actual period.

In DIANA, a slightly different approach is used. Module STRDYN offers a *multiple* shooting method, in which time interval $[0, T\rangle$ is subdivided into n_{sh}

sections of equal length. In all these sections, a shooting method is applied, implying, that zeros of a different function $\underset{\sim}{H}$ must be found. In this report, however, *simple* shooting is used ($n_{\mathrm{sh}} = 1$), so (2.3) is still valid.

In DIANA, state $\underset{\sim}{x}$ is defined by a column $\underset{\sim}{q}$, with the positions of the system, and a column $\dot{\underset{\sim}{q}}$, with the first time derivatives of these positions, as

$$\underset{\sim}{x} = \begin{bmatrix} \underset{\sim}{q} \\ \dot{\underset{\sim}{q}} \end{bmatrix}. \tag{2.9}$$

To make (2.3) solvable, in STRDYN, one of the components of $\dot{\underset{\sim}{q}}$ is set to zero. Here it is assumed to be the last one, giving $\underset{\sim}{x} = [\ \underset{\sim}{x}_{\mathrm{a}}^{\mathrm{T}}\ \ 0\ ]^{\mathrm{T}}$. This is substituted in (2.3), to obtain

$$\underset{\sim}{H}(\underset{\sim}{z}) \equiv \underset{\sim}{\phi}_T\left(\begin{bmatrix} \underset{\sim}{x}_{\mathrm{a}} \\ 0 \end{bmatrix}\right) - \begin{bmatrix} \underset{\sim}{x}_{\mathrm{a}} \\ 0 \end{bmatrix} = \underset{\sim}{0}, \tag{2.10}$$

where $\underset{\sim}{z} = [\ \underset{\sim}{x}_{\mathrm{a}}^{\mathrm{T}}\ \ T\ ]^{\mathrm{T}}$. This system of equations can be solved with the Newton–Raphson algorithm, using initial guess $\underset{\sim}{z}^{(0)}$.

Unfortunately, STRDYN does not perform a minimum period test on the calculated solution.

2.3 Path following

In the path following algorithm (taken from Fey [4]), it is investigated, how varying a design variable r influences a periodic solution. The parameterized state equation is given by

$$\dot{\underset{\sim}{x}} = \underset{\sim}{f}(\underset{\sim}{x}, r). \tag{2.11}$$

When path following is performed, together with the simple shooting method, solutions are calculated of

$$\underset{\sim}{h}(\underset{\sim}{z}, r) \equiv \underset{\sim}{\phi}_T\left(\begin{bmatrix} \underset{\sim}{x}_{\mathrm{a}} \\ 0 \end{bmatrix}, r\right) - \begin{bmatrix} \underset{\sim}{x}_{\mathrm{a}} \\ 0 \end{bmatrix} = \underset{\sim}{0}, \tag{2.12}$$

where, again, $\underset{\sim}{z} = [\ \underset{\sim}{x}_{\mathrm{a}}^{\mathrm{T}}\ \ T\ ]^{\mathrm{T}}$ and $\underset{\sim}{x} = [\ \underset{\sim}{x}_{\mathrm{a}}^{\mathrm{T}}\ \ 0\ ]^{\mathrm{T}}$. As before, the last component of $\underset{\sim}{x}$ is set to zero.

First, a periodic solution $[\ \underset{\sim}{z}_{\mathrm{s},1}^{\mathrm{T}}\ \ r_{\mathrm{s},1}\ ]^{\mathrm{T}}$ must be calculated, using the shooting method. Then, starting from this solution, a branch of solutions can be followed, by means of a predictor—corrector mechanism. In Fig. 2.1 this mechanism is shown for one path following step.

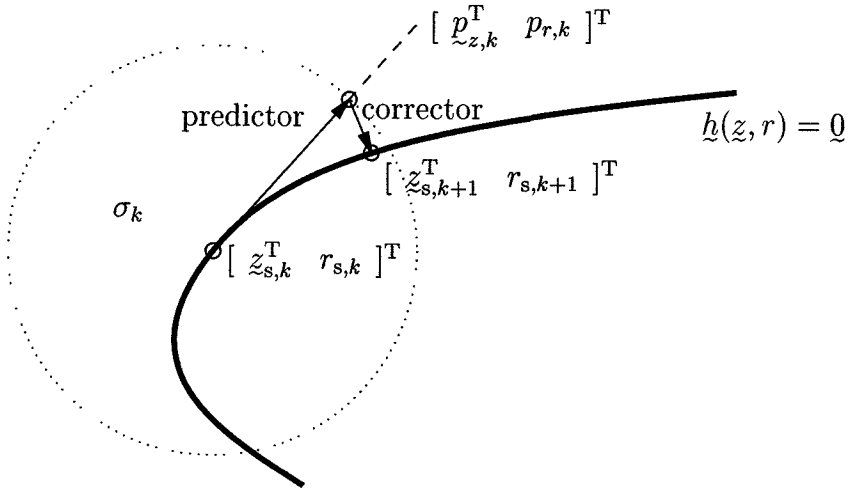

Figure 2.1: Path following step k

In predictor step k, the tangent $[\ \underset{\sim}{p}_{z,k}^{\mathrm{T}}\quad p_{r,k}\ ]^{\mathrm{T}}$ to the solution branch at $[\ \underset{\sim}{z}_{\mathrm{s},k}^{\mathrm{T}}\quad r_{\mathrm{s},k}\ ]^{\mathrm{T}}$ is determined by linearizing (2.12), giving

$$\frac{\partial \underline{h}}{\partial \underset{\sim}{z}} \underset{\sim}{p}_{z,k} + \frac{\partial \underline{h}}{\partial r} p_{r,k} = \underline{0}. \tag{2.13}$$

In the first predictor step, $p_{r,1}$ is set to 1, if r must be increased initially, and to -1, if r must be decreased initially. In subsequent steps, $p_{r,k}$ can be set to 1, so (2.13) can be solved for $\underset{\sim}{p}_{z,k}$. The tangent is scaled by a factor $\sigma_{p,k}$, derived from the elliptical constraint

$$\sigma_{p,k}^2 (\underset{\sim}{p}_{z,k}^{\mathrm{T}} \underset{\sim}{p}_{z,k} + p_{r,k}^2) = \sigma_k^2, \tag{2.14}$$

where σ_k is the step size, that lies in a user defined interval,

$$0 < \sigma_{\min} \leq \sigma_k \leq \sigma_{\max}. \tag{2.15}$$

In step $k > 1$, the sign of $\sigma_{p,k}$ is chosen such, that the scaled tangents of two succeeding predictor steps form an acute angle. This is achieved by requiring, that

$$\operatorname{sgn}(\sigma_{p,k}) = \operatorname{sgn}[\sigma_{p,k-1} (\underset{\sim}{p}_{z,k-1}^{\mathrm{T}} \underset{\sim}{p}_{z,k} + p_{r,k-1} p_{r,k})]. \tag{2.16}$$

This ensures, that a solution branch is followed in the same direction, all the time. In Fig. 2.1 the elliptical constraint is represented by the dotted circle, with radius σ_k. The prediction $[\ \underset{\sim}{z}_{\mathrm{p},k}^{\mathrm{T}}\quad r_{\mathrm{p},k}\ ]^{\mathrm{T}}$ is given by

$$\begin{bmatrix} \underset{\sim}{z}_{\mathrm{p},k} \\ r_{\mathrm{p},k} \end{bmatrix} = \begin{bmatrix} \underset{\sim}{z}_{\mathrm{s},k} \\ r_{\mathrm{s},k} \end{bmatrix} + \sigma_{p,k} \begin{bmatrix} \underset{\sim}{p}_{z,k} \\ p_{r,k} \end{bmatrix}. \tag{2.17}$$

In general, this prediction will not meet the convergence criterion, that is used, and an iterative correction process will be needed.

Corrector step m is given by

$$\begin{bmatrix} \underset{\sim}{z}_{c,k,m+1} \\ r_{c,k,m+1} \end{bmatrix} = \begin{bmatrix} \underset{\sim}{z}_{c,k,m} \\ r_{c,k,m} \end{bmatrix} + \begin{bmatrix} \underset{\sim}{c}_{z,k,m} \\ c_{r,k,m} \end{bmatrix}. \tag{2.18}$$

In the first corrector step, the first term on the right hand side of this equation is set equal to the prediction from (2.17). Corrections are calculated by solving the following system of equations, which is similar to the Newton–Raphson algorithm.

$$\begin{bmatrix} \dfrac{\partial \underset{\sim}{h}}{\partial \underset{\sim}{z}} & \dfrac{\partial \underset{\sim}{h}}{\partial r} \\ -\left(\left(\dfrac{\partial \underset{\sim}{h}}{\partial \underset{\sim}{z}}\right)^{-1} \dfrac{\partial \underset{\sim}{h}}{\partial r}\right)^{\mathrm{T}} & 1 \end{bmatrix} \begin{bmatrix} \underset{\sim}{c}_{z,k,m} \\ c_{r,k,m} \end{bmatrix} = \begin{bmatrix} -\underset{\sim}{h} \\ 0 \end{bmatrix} \tag{2.19}$$

In these equations, $\underset{\sim}{h}$, $\partial \underset{\sim}{h}/\partial \underset{\sim}{z}$ and $\partial \underset{\sim}{h}/\partial r$ are evaluated at $[\ \underset{\sim}{z}_{c,k,m}^{\mathrm{T}} \quad r_{c,k,m}\ ]^{\mathrm{T}}$ and the last equation forces the corrections to be orthogonal to the solution space. The corrected term $[\ \underset{\sim}{z}_{c,k,m+1}^{\mathrm{T}} \quad r_{c,k,m+1}\ ]^{\mathrm{T}}$ from (2.18) is accepted as the next solution $[\ \underset{\sim}{z}_{s,k+1}^{\mathrm{T}} \quad r_{s,k+1}\ ]^{\mathrm{T}}$, if the convergence criterion is met.

Changes in step size σ_k are determined by the ratio between the Euclidean norms of the corrections in path following steps $k-1$ and $k-2$. If this ratio is lower than a used defined minimum, the step size will be increased. As soon as it exceeds a user defined maximum, the step size will be decreased and the last prediction will be recalculated, using the new step size. Furthermore, during the iterative correction process, it is required, that the norm of the residue is decreased monotonically, that is

$$\|\underset{\sim}{h}(\underset{\sim}{z}_{c,k,m+1}, r_{c,k,m+1})\| < \|\underset{\sim}{h}(\underset{\sim}{z}_{c,k,m}, r_{c,k,m})\|. \tag{2.20}$$

If this inequality is violated, the last prediction will be rejected and a new prediction will be calculated, using a smaller step size.

If the step size is too large, the path following algorithm may change the direction, in which a solution branch is followed, due to (2.16). This often occurs in areas, where the solution branch is very curved. It can be prevented, by requiring, that angle β_1, between the scaled tangent at path following step k and the line, pointing from solution k to solution $k+1$, is smaller than a user defined maximum $\beta_{1,\max}$, where

$$\beta_1 = \arccos \frac{\sigma_{p,k}[\ \underset{\sim}{p}_{z,k}^{\mathrm{T}} \quad p_{r,k}\ ]([\ \underset{\sim}{z}_{s,k+1}^{\mathrm{T}} \quad r_{s,k+1}\ ]^{\mathrm{T}} - [\ \underset{\sim}{z}_{s,k}^{\mathrm{T}} \quad r_{s,k}\ ]^{\mathrm{T}})}{\|\sigma_{p,k}[\ \underset{\sim}{p}_{z,k}^{\mathrm{T}} \quad p_{r,k}\ ]^{\mathrm{T}}\|\|[\ \underset{\sim}{z}_{s,k+1}^{\mathrm{T}} \quad r_{s,k+1}\ ]^{\mathrm{T}} - [\ \underset{\sim}{z}_{s,k}^{\mathrm{T}} \quad r_{s,k}\ ]^{\mathrm{T}}\|}. \tag{2.21}$$

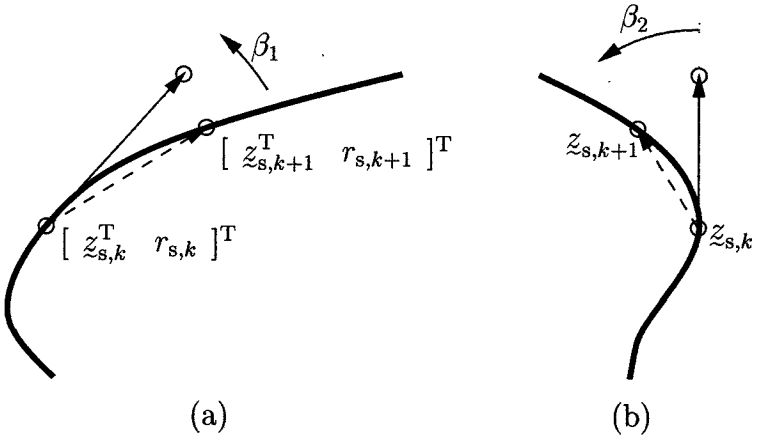

Figure 2.2: (a) Angle β_1, (b) angle β_2

Furthermore, it is possible, that the path following algorithm jumps over to another branch or a remote part of the same branch, if the step size is too large. This can usually be prevented, by requiring, that angle β_2, between the projections onto an $(n-1)$-dimensional hyper plane, perpendicular to the r–axis, of the scaled tangent at step k and the line pointing from solution k to solution $k+1$, is smaller than a user defined maximum $\beta_{2,\max}$, where

$$\beta_2 = \arccos \frac{\sigma_{p,k} p_{z,k}^T (z_{s,k+1} - z_{s,k})}{\|\sigma_{p,k} p_{z,k}\| \|(z_{s,k+1} - z_{s,k})\|}. \tag{2.22}$$

If, at path following step k, $\beta_1 > \beta_{1,\max}$ or $\beta_2 > \beta_{2,\max}$, solution $k+1$ will be rejected and a new prediction will be calculated, using a smaller step size. In Figs. 2.2(a) and (b), angles β_1 and β_2 are depicted, respectively.

The path following algorithm fails, when (a), σ_k becomes smaller than $\sigma_{\min}$, (b), the iterative correction process does not converge or (c), a dynamic bifurcation point is encountered. In a dynamic bifurcation point, namely, one of the matrices

$$\frac{\partial h}{\partial z} \text{ and } \frac{\partial h}{\partial z} + \frac{\partial h}{\partial r} \left(\left(\frac{\partial h}{\partial z} \right)^{-1} \frac{\partial h}{\partial r} \right)^T \tag{2.23}$$

becomes singular, so (2.13) or (2.19) can not be solved.

2.4 Stability

The local stability of a periodic solution $\phi_t(\hat{x})$, with period time $\hat{T}$, is investigated by linearizing (2.1) and examining the evolution in time of an

infinitesimal initial perturbation $\delta\underset{\sim}{x}_0$ of $\hat{\underset{\sim}{x}}$. It follows, that to first order,

$$\delta\dot{\underset{\sim}{x}} = \underline{A}(t)\delta\underset{\sim}{x}, \qquad \delta\underset{\sim}{x}(t=0) = \delta\underset{\sim}{x}_0, \tag{2.24}$$

where $\underline{A}(t) \equiv \mathrm{d}\underset{\sim}{f}/\mathrm{d}\underset{\sim}{x}$, evaluated at $\hat{\underset{\sim}{x}}$, and $\underline{A}(t) = \underline{A}(t+\hat{T})$, because of the periodicity of $\underset{\sim}{\phi}_t(\hat{\underset{\sim}{x}})$. In appendix A it is shown, that

$$\delta\underset{\sim}{x}(t) = \underline{\Phi}_t(\hat{\underset{\sim}{x}})\delta\underset{\sim}{x}_0. \tag{2.25}$$

According to Floquet's theory, matrix $\underline{\Phi}_t(\hat{\underset{\sim}{x}})$ satisfies the condition

$$\underline{\Phi}_{t+\hat{T}}(\hat{\underset{\sim}{x}}) = \underline{\Phi}_t(\hat{\underset{\sim}{x}})\underline{\Phi}_{\hat{T}}(\hat{\underset{\sim}{x}}), \tag{2.26}$$

where $\underline{\Phi}_{\hat{T}}(\hat{\underset{\sim}{x}}) = \underline{\Phi}_\lambda$ is a constant, regular matrix, called the monodromy matrix. Using this property, it can easily be shown, that

$$\underline{\Phi}_t(\hat{\underset{\sim}{x}}) = \underline{\Phi}_{t^*}(\hat{\underset{\sim}{x}})\underline{\Phi}_\lambda^k, \tag{2.27}$$

where $t^* = t - k\hat{T}$, $0 \leq t^* < \hat{T}$ and $k \in \mathbb{Z}$. Substituting this equation in (2.25) gives, since $\underline{\Phi}_0(\hat{\underset{\sim}{x}}) = \underline{I}$,

$$\delta\underset{\sim}{x}(k\hat{T}) = \underline{\Phi}_\lambda^k\delta\underset{\sim}{x}_0. \tag{2.28}$$

Monodromy matrix $\underline{\Phi}_\lambda$ has eigenvalues λ_i, where $|\lambda_i| \geq |\lambda_{i+1}|$ $(i = 1,\ldots,n)$, called the *Floquet multipliers.* They determine the long term behavior of perturbation $\delta\underset{\sim}{x}(t)$ and, therefore, the local stability of periodic solution $\underset{\sim}{\phi}_t(\hat{\underset{\sim}{x}})$. Because, in an autonomous system, the phase of the solution is undefined, one of the Floquet multiplier always equals 1. Referring to (2.28), the stability conditions are given by

	STABILITY
$\lvert\lambda_i < 1\rvert$, $i = 2,\ldots,n$,	(asymptotically) stable,
$\lvert\lambda_2\rvert = 1$,	marginally stable,
$\lvert\lambda_1\rvert > 1$,	unstable.

Chapter 3

Examples

Before going to the drill string model, in this chapter some example systems are discussed. First, the well known Van der Pol equation is treated. This equation represents an autonomous system, displaying a self-sustained oscillation, analogous to the stick—slip vibration of the drill string. It is dealt with here, to show, how such systems are analyzed with STRDYN. To determine, if dry friction can be modeled in DIANA, some results of 1– and 2–DOF dry friction models, found in literature, are reproduced. MATLAB is used, to find semi-analytic solutions of the 1–DOF dry friction model, applying Hénon's method. These solutions are used, to estimate the errors in the DIANA results.

3.1 Van der Pol equation

3.1.1 Shooting

The nondimensional Van der Pol equation is given by the state equation

$$\dot{\underset{\sim}{x}} = \underset{\sim}{f}(\underset{\sim}{x}) = \begin{bmatrix} \dot{x} \\ -\nu(x^2 - 1)\dot{x} - x \end{bmatrix}, \tag{3.1}$$

where a dot ($\dot{}$) denotes a differentiation to nondimensional time t, $\underset{\sim}{x} = [\ x \quad \dot{x}\ ]^{\mathrm{T}}$, and $\nu > 0$.

The simple shooting method with Runge–Kutta–Fehlberg integration is used to determined a periodic solution. Parameter ν is taken equal to 1. To achieve convergence, an accurate initial guess is required, which can be obtained by integrating (3.1) from an arbitrary initial condition, until the transient is damped out. Fig. 3.1 shows the familiar limit cycle, that is calculated with initial guess $\underset{\sim}{z}^{(0)} = [\ x^{(0)} \quad T^{(0)}\ ] = [\ 2.0082 \quad 6.6634\ ]$. The

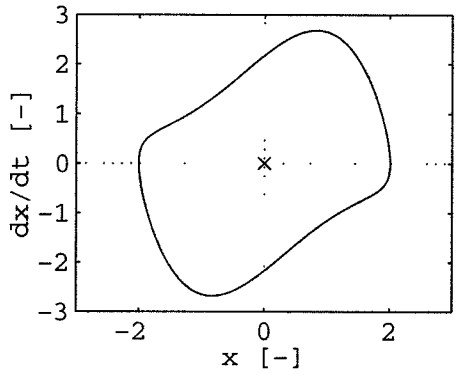

Figure 3.1: Limit cycle at $\nu = 1$

Floquet multipliers of this solution are given by $\lambda_1 = 1$ and $\lambda_2 = 0.8597 \cdot 10^{-3}$, so the limit cycle is stable, which is obvious, because integration is used to determine the initial guess. This implies, that the path following algorithm is usually started from stable solutions.

It is noted, that, in addition to the limit cycle, an unstable equilibrium point, located at $\underset{\sim}{x}_{eq} = [\ 0 \quad 0\ ]^T$, exists for all values of ν. Equilibrium points are the zeros of $\underset{\sim}{f}$. Their stability is determined by the eigenvalues of $\mathrm{d}\underset{\sim}{f}/\mathrm{d}\underset{\sim}{x}$, evaluated at $\underset{\sim}{x}_{eq}$. In this case the eigenvalues have positive real parts. In Fig. 3.1 the equilibrium point is depicted by the x–mark ($\times$). Unfortunately, module STRDYN does not offer a possibility for finding equilibrium points. The shooting method, however, sometimes converges to an equilibrium point, returning a senseless period time.

3.1.2 Path following

Parameter ν is used as the design variable in path following. With the calculated limit cycle at $\nu = 1$ as the initial solution, the design variable is first decreased from 1 to 0 and subsequently increased from 1 to 15. The calculations took about 15 minutes of CPU time. In Fig. 3.2, the absolute maxima of x ($\max|x|$) and $\dot{x}$ ($\max|\dot{x}|$) of the periodic solutions are plotted against ν. The absolute maximum of x is approximately 2 for all values of ν, whereas the absolute maximum of $\dot{x}$ increases almost linearly from 2 at $\nu = 0$ to about 20 at $\nu = 15$. These characteristics are also found in literature. The unexpected oscillation in the absolute maximum of $\dot{x}$, for $\nu > 10$, is caused by the discretization of the periodic solution by the numerical integration method. Because of sharp peaks in the velocity, the approximation of its maximum is not accurate. Increasing the number of output points will reduce this effect, but has a negative influence on CPU time. The free frequency and

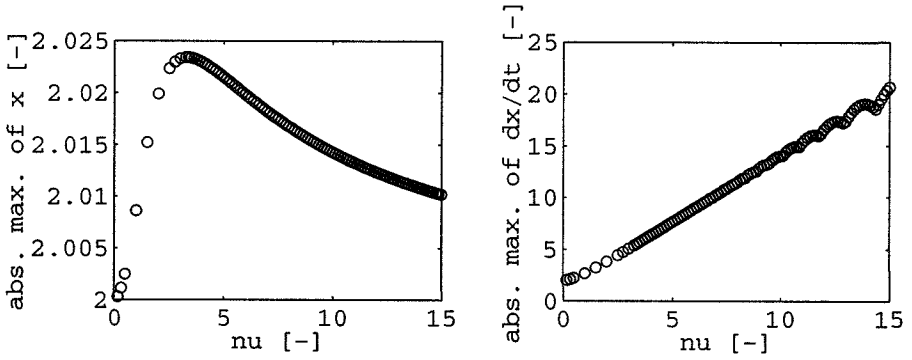

Figure 3.2: Absolute maxima of x and $\dot{x}$

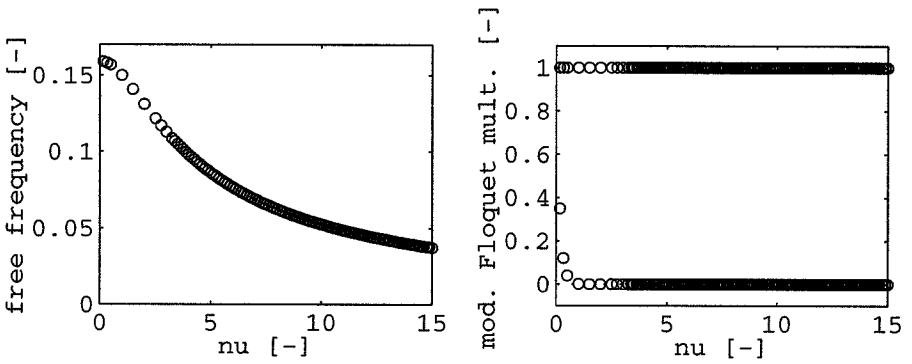

Figure 3.3: Free frequency and moduli of Floquet multipliers

the moduli of the Floquet multipliers are given in Fig. 3.3. It can be seen, that if $\nu \downarrow 0$, the free frequency approaches $1/2\pi \approx 0.16$, which corresponds to the eigenfrequency of the linear system, where $\nu = 0$. If $\nu \to \infty$, the free frequency approaches 0, which is also known from literature. According to the Floquet multipliers, all solutions are stable. If $\nu \downarrow 0$, the modulus of Floquet multiplier λ_2 approaches 1, indicating a marginally stable solution, which again corresponds to the linear system.

3.1.3 Conclusions

The results, found with DIANA, correspond to what is found in literature. The shooting method requires an accurate guess, to achieve convergence. Because of discretization, inconsistencies can occur in the results. Equilibrium points can not be found by module STRDYN.

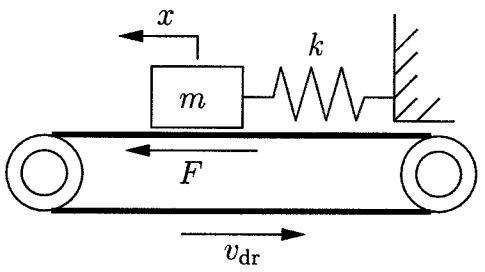

Figure 3.4: 1–DOF model with dry friction

3.2 1–DOF dry friction model

3.2.1 Shooting

A 1–DOF model with dry friction (taken from Galvanetto *et al.* [5]), is depicted in Fig. 3.4. Mass m is attached to inertial space by spring k, where $m = 1$ [kg] and $k = 1$ [N/m]. The mass is riding on a driving belt, that is moving at a constant velocity v_{dr}. Between the mass and the belt, dry friction occurs, with a friction force F. The state equation, describing this model, reads

$$\dot{\underset{\sim}{x}} = \underset{\sim}{f}(\underset{\sim}{x}) = \begin{bmatrix} \dot{x} \\ -\dfrac{k}{m}x + \dfrac{F}{m} \end{bmatrix}, \tag{3.2}$$

where a dot ($\dot{}$) denoted a differentiation to time t, $\underset{\sim}{x} = [\ x \quad \dot{x}\ ]$ and F is given by

$$\begin{cases} |F| \leq \mu_0 F_{\text{N}}, & v_{\text{rel}} = 0, \\ F = -\mu F_{\text{N}} \operatorname{sgn} v_{\text{rel}}, & v_{\text{rel}} \neq 0. \end{cases} \tag{3.3}$$

$F_{\text{s}} = \mu_0 F_{\text{N}}$ is the maximum static friction force and is chosen equal to 1 [N], whereas $v_{\text{rel}} = \dot{x} - v_{\text{dr}}$ is the relative velocity of mass m with respect to the belt. The dynamic friction coefficient $\mu = \mu(|v_{\text{rel}}|)$ is given by

$$\mu = \frac{\mu_0}{1 + \delta|v_{\text{rel}}|}. \tag{3.4}$$

Positive parameter δ measures the rate, at which μ decreases, with an increase in $|v_{\text{rel}}|$, and is taken equal to 3 [s/m]. Using this, (3.3) can be rewritten as

$$\begin{cases} |F| \leq F_{\text{s}}, & v_{\text{rel}} = 0, \\ F = -\dfrac{F_{\text{s}} \operatorname{sgn} v_{\text{rel}}}{1 + \delta|v_{\text{rel}}|}, & v_{\text{rel}} \neq 0. \end{cases} \tag{3.5}$$

Fig. 3.5 shows the friction force as a function of the relative velocity. F is discontinuous at $v_{\text{rel}} = 0$ and, therefore, causes the differential equation to be

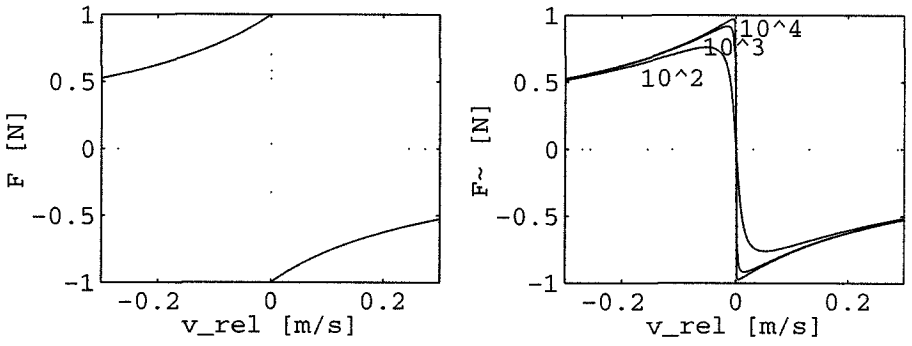

Figure 3.5: Friction force F and the approximation $\tilde{F}$

highly nonlinear. To avoid numerical problems in STRDYN, the friction force must be approximated by a smooth $\tilde{F}$. This can be achieved by dropping the first equation of (3.5) and substituting $\operatorname{sgn} v_{\text{rel}}$ in the second equation with $(2/\pi)\arctan \varepsilon v_{\text{rel}}$, to obtain

$$\tilde{F} = -\frac{F_s \frac{2}{\pi} \arctan \varepsilon v_{\text{rel}}}{1 + \delta |v_{\text{rel}}|}. \tag{3.6}$$

Fig. 3.5 shows $\tilde{F}$ as a function of v_{rel}, for some values of ε ($\varepsilon = 10^2$, 10^3 and 10^4). Clearly, increasing ε improves to approximation, especially for v_{rel} close to 0. However, a steep slope in $\tilde{F}$ is created at $v_{\text{rel}} = 0$, given by $-(2/\pi)\varepsilon F_s$. This causes a stiff differential equation, so the BDF (backward differentiation formula, see Hindmarsh [7]) method is used for numerical integration.

In Fig. 3.6 the stable periodic solution at $v_{\text{dr}} = 0.2$ [m/s] is shown, calculated with the simple shooting method, for different values of ε ($\varepsilon = 10^i$, $i = 2, \ldots, 7$)[1]. The circles (o) represent a semi-analytic solution, that is found with MATLAB, without approximating the friction force. This solution is obtained, using simple shooting and applying Hénon's method [6], to integrate over the discontinuity with a 4th-order Runge–Kutta scheme.

The relative errors in the absolute maximum of x and the free frequency of a solution, calculated with DIANA can now be expressed as

$$e_x(\varepsilon) = \left| \frac{\max |x(\varepsilon)| - \max |x_{\text{exact}}|}{\max |x_{\text{exact}}|} \right|, \tag{3.7}$$

$$e_f(\varepsilon) = \left| \frac{f(\varepsilon) - f_{\text{exact}}}{f_{\text{exact}}} \right|, \tag{3.8}$$

where $\max |x(\varepsilon)|$ and $\max |x_{\text{exact}}|$ are the absolute maxima of x of the DIANA solution and the semi-analytic MATLAB solution, respectively, whereas $f(\varepsilon)$

[1]Some parts of the DIANA user subroutines, used in this report, are given in appendix B

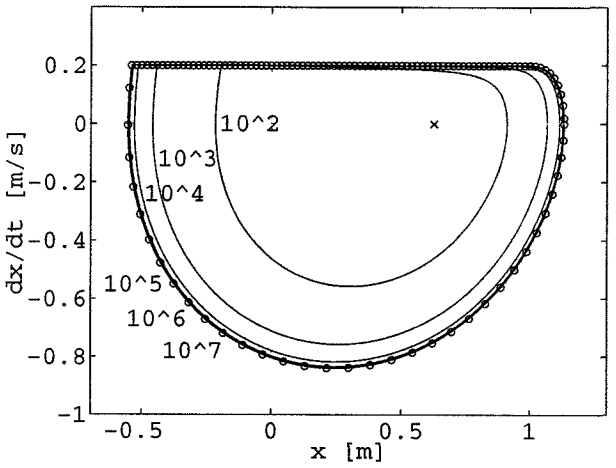

Figure 3.6: Periodic solutions at $v_{\mathrm{dr}} = 0.2$ [m/s]

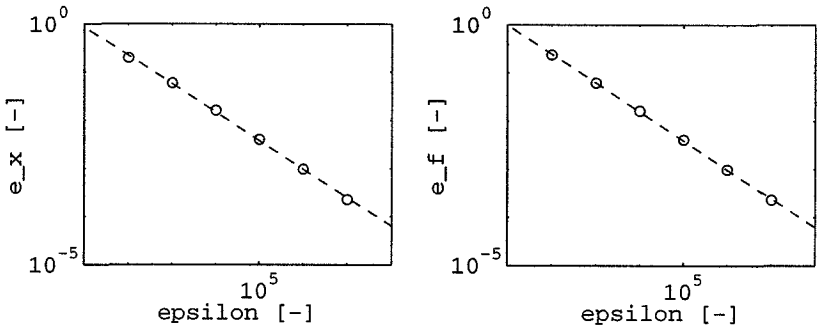

Figure 3.7: Errors e_x and e_f for $v_{\mathrm{dr}} = 0.2$ [m/s]

and f_{exact} are the free frequencies of these solutions. In Fig. 3.7, the errors at $v_{\mathrm{dr}} = 0.2$ [m/s] are plotted with circles (o), using double logarithmic scales. The dashed lines in this figure are least squares fits with function $e(\varepsilon) = b\varepsilon^a$, where a and b are given in the next table.

	e_x	e_f
a	-0.59	-0.60
b	3.3	3.9

So, a relative accuracy of, for instance, 10^{-3} is achieved by choosing $\varepsilon \geq 9.7 \cdot 10^5$, based on e_f.

Like the Van der Pol equation, this system possesses an unstable equilibrium point. It is given by $\underset{\sim}{x}_{\mathrm{eq}} = [\ F/k \quad 0\ ]^{\mathrm{T}}$, where $F = F_{\mathrm{s}}/(1+\delta v_{\mathrm{dr}}) = 1/(1+3v_{\mathrm{dr}})$, if $v_{\mathrm{dr}} > 0$. In Fig. 3.6 the equilibrium point at $v_{\mathrm{dr}} = 0.2$ [m/s] is represented by the x-mark ($\times$) at $\underset{\sim}{x}_{\mathrm{eq}} = [\ 0.625 \quad 0\ ]^{\mathrm{T}}$. In the approximated

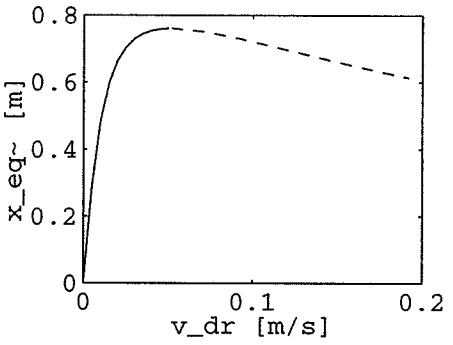

Figure 3.8: Equilibrium point $\tilde{x}_{\text{eq}}$ ($\varepsilon = 10^2$)

system, however, the equilibrium point is located at

$$\tilde{\underset{\sim}{x}}_{\text{eq}} = \begin{bmatrix} \tilde{x}_{\text{eq}} \\ 0 \end{bmatrix} = \begin{bmatrix} \frac{2}{\pi} \arctan \varepsilon v_{\text{dr}} \\ 1 + 3v_{\text{dr}} \\ 0 \end{bmatrix}. \tag{3.9}$$

When v_{dr} is decreased below some value $v_{\text{bif}} = v_{\text{bif}}(\varepsilon)$, this equilibrium point becomes stable, because the eigenvalues of $\partial \underset{\sim}{f} / \partial \underset{\sim}{x}$ cross the imaginary axis and get negative real parts. This does not correspond to the original system, where the equilibrium point is always unstable. Fig. 3.8 shows $\tilde{x}_{\text{eq}}$ as a function of v_{dr}, for $\varepsilon = 10^2$, where $v_{\text{bif}} \approx 0.052$. The solid line represents the stable equilibrium points, the dashed line unstable ones.

3.2.2 Path following

The velocity of the driving belt is used as the design variable and is decreased from 0.2 [m/s] towards 0. Again, the calculations are repeated for different values of ε ($\varepsilon = 10^i$, $i = 2, \ldots, 7$). An average of about 10 minutes of CPU time are needed per branch. Figs. 3.9 and 3.10 show the absolute maximum of x and the free frequency of the periodic solutions. The branches do not reach $v_{\text{dr}} = 0$, because the step size becomes less than a user defined minimum.

If $v_{\text{dr}} \downarrow 0$, the absolute maximum of x should approach 1, because the stick phase ends at $x = F_{\text{s}}/k = 1$, when the elastic force of the spring equals the maximum static friction force. Looking at figure 3.6, the limit cycle will cross the x–axis at approximately $\underset{\sim}{x} = [\ 1 \quad 0\ ]^{\text{T}}$, when $v_{\text{dr}} \approx 0$. The free frequency should approach 0, because of a longer stick phase at low driving belt velocities. Clearly, a larger value of ε gives a better correspondence to these conditions. It is also noted, that for all values of ε, the limit cycle vanishes, if v_{dr} is decreased below v_{bif}. This does not correspond to the original system, where a limit cycle exists for all values of $v_{\text{dr}} \neq 0$.

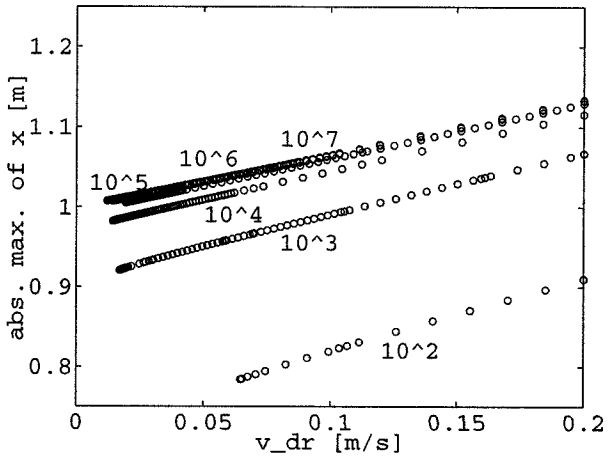

Figure 3.9: Absolute maximum of x

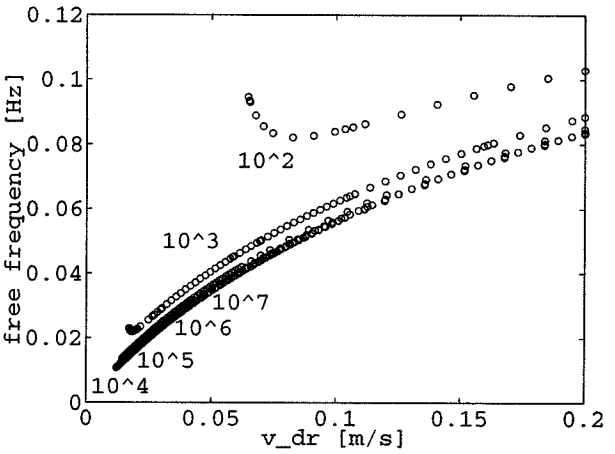

Figure 3.10: Free frequency

The eigenfrequency of the linear system, without dry friction, is equal to $1/2\pi \approx 0.16$. It seems, that this value is approached by the free frequency, if $v_{\mathrm{dr}} \to \infty$.

Unfortunately, DIANA does not correctly interpret the Floquet multipliers of the calculated solutions. Due to numerical errors, the Floquet multiplier, that should be equal to 1, is sometimes estimated slightly greater than 1, causing STRDYN to label a solution unstable, while it is stable. Therefore, MATLAB is used to post-process the DIANA results, concluding that the periodic solutions on all branches are stable.

Again, MATLAB is used, to calculate semi-analytic solutions at $v_{\mathrm{dr}} = 0.05$, 0.1 and 0.15 [m/s] and parameters a and b of the relative errors are

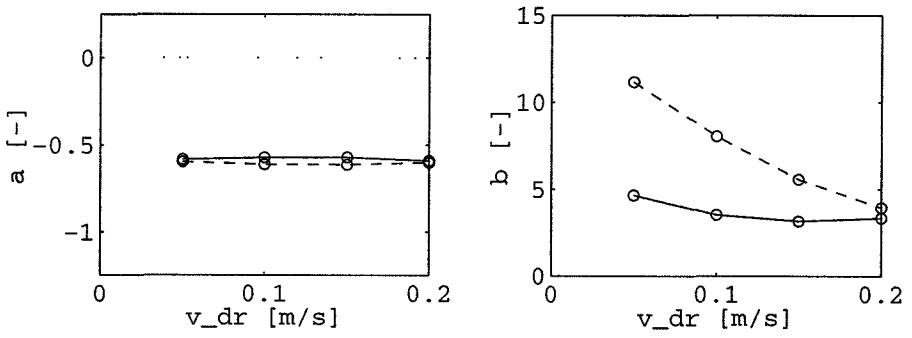

Figure 3.11: Parameters a and b

determined. In Fig. 3.11, a and b are shown, as functions of v_{dr}. The solid lines belong to error e_x, the dashed lines to e_f. It can be seen, that a is approximately constant, but b increases, when the velocity of the belt is decreased. Also, a is about equal for both e_x and e_f, whereas b is larger for e_f than for e_x. Therefore, the choice of parameter ε should be based on the error in the free frequency at the smallest value of v_{dr}, that is of interest. The parameters of e_x and e_f, at different values of v_{dr}, are given in the next table.

	v_{dr}	0.05	0.1	0.15	0.2
e_x	a	-0.58	-0.57	-0.57	-0.59
	b	4.7	3.5	3.2	3.3
e_f	a	-0.60	-0.61	-0.61	-0.60
	b	11	8.1	5.6	3.9

3.2.3 Conclusions

In STRDYN, it is not possible to use Hénon's method. Therefore, the discontinuous friction force must be approximated by a smooth function. It is concluded, that satisfactory results can be achieved, by approximating the friction force, using an arctan–function. Due to numerical errors, DIANA does not determine the stability of solutions of autonomous systems correctly. The required accuracy of the calculated solutions should be defined at the lowest driving belt velocity of interest.

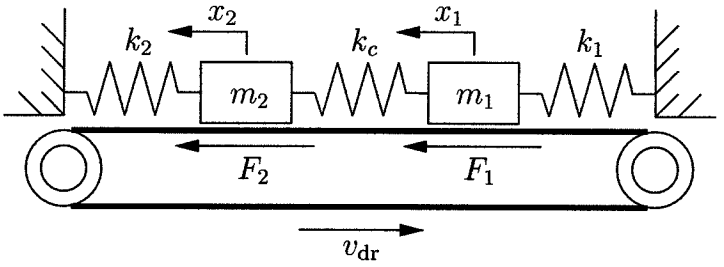

Figure 3.12: 2–DOF model with dry friction

3.3 2–DOF dry friction model

3.3.1 Shooting

A 2–DOF model with dry friction (also taken from Galvanetto *et al.* [5]), is shown in Fig. 3.12. Two masses, m_1 and m_2, are riding on a driving belt, that is moving at a constant velocity v_{dr}. These masses are connected by a spring k_c, while m_1 and m_2 are attached to inertial space by k_1 and k_2, respectively. Between the masses and the belt, dry friction occurs, with friction forces F_1 and F_2. It is assumed that $m_1 = m_2 = m$ and $k_1 = k_2 = k$. The nondimensional state equation is given by

$$\dot{\underset{\sim}{x}} = \underset{\sim}{f}(\underset{\sim}{x}) = \begin{bmatrix} \dot{X}_1 \\ -X_1 - \alpha(X_1 - X_2) + f_1 \\ \dot{X}_2 \\ -X_2 - \alpha(X_2 - X_1) + f_2 \end{bmatrix}, \tag{3.10}$$

where $\underset{\sim}{x} = [\ X_1 \quad \dot{X}_1 \quad X_2 \quad \dot{X}_2\ ]^{\mathrm{T}}$,

$$\begin{cases} |f_1| \le 1, & V_{\mathrm{rel},1} = 0, \\ f_1 = -\dfrac{\operatorname{sgn} V_{\mathrm{rel},1}}{1 + \gamma |V_{\mathrm{rel},1}|}, & V_{\mathrm{rel},1} neq 0, \end{cases} \tag{3.11}$$

$$\begin{cases} |f_2| \le \beta & V_{\mathrm{rel},2} = 0, \\ f_2 = -\dfrac{\beta \operatorname{sgn} V_{\mathrm{rel},2}}{1 + \gamma |V_{\mathrm{rel},2}|}, & V_{\mathrm{rel},2} \neq 0, \end{cases} \tag{3.12}$$

$V_{\mathrm{rel},i} = \dot{X}_i - V_{\mathrm{dr}}$ $(i = 1, 2)$, a dot $(\dot{})$ denotes a differentiation to τ, $\tau = t\sqrt{k/m}$ (t is time), $X_i = x_i k / F_{\mathrm{s}1}$, $\alpha = k_c/k$, $\beta = F_{\mathrm{s}2}/F_{\mathrm{s}1}$ and $V_{\mathrm{dr}} = (\sqrt{km} v_{\mathrm{dr}})/F_{\mathrm{s}1}$. $F_{\mathrm{s}i}$ is the maximum static friction force on mass m_i $(i = 1, 2)$. The following values are chosen.

$$\alpha = 1.2, \quad \beta = 1.3, \quad \gamma = 3 \tag{3.13}$$

In the calculations, carried out with DIANA, the first equations of (3.11) and (3.12) are dropped and in the second equations, $\operatorname{sgn} V_{\mathrm{rel},i}$ is substituted by $(2/\pi)\arctan \varepsilon V_{\mathrm{rel},i}$ $(i = 1, 2)$. Here, $\varepsilon = 10^5$ is used initially, to obtain an accuracy of about $11 \cdot (10^5)^{-0.60} = 0.011$ at $V_{\mathrm{dr}} = 0.05$.

Simple shooting with BDF integration is used to determine periodic solutions. Figs. 3.13 and 3.14 show some stable solutions at different values of V_{dr}, that are used as initial solutions for the path following calculations in the next subsection. In these figures, X_2 is plotted against X_1. The solutions in Fig. 3.13 show the two masses oscillating 'in phase'. That is, masses m_1 and m_2 are roughly moving in the same direction. In this figure, period-2, -1 and -2 solutions are plotted, at $V_{\mathrm{dr}} = 0.08$, 0.14 and 0.15, respectively. A period-n solution is defined as a periodic solution, that crosses the Poincaré section, given by $\dot{X}_1 = 0$, n times from negative to positive, during its minimum period time. Fig. 3.14 shows some 'out of phase' solutions, where masses m_1 and m_2 are roughly moving in opposite directions. In this figure, period-8, -4, -2 and -1 solutions are plotted, at $V_{\mathrm{dr}} = 0.127$, 0.14, 0.2 and 0.35, respectively.

The unstable equilibrium point of this system is given by

$$x_{\mathrm{eq}} = \begin{bmatrix} \dfrac{1+\alpha+\alpha\beta}{(1+2\alpha)(1+\gamma V_{\mathrm{dr}}} \\ 0 \\ \dfrac{\alpha+\beta+\alpha\beta}{(1+2\alpha)(1+\gamma V_{\mathrm{dr}}} \\ 0 \end{bmatrix} = \begin{bmatrix} \dfrac{3.76}{3.4(1+3V_{\mathrm{dr}})} \\ 0 \\ \dfrac{4.06}{3.4(1+3V_{\mathrm{dr}})} \\ 0 \end{bmatrix}. \tag{3.14}$$

In the approximated system, the equilibrium point is located at

$$\tilde{x}_{\mathrm{eq}} = \begin{bmatrix} \dfrac{3.76\frac{2}{\pi}\arctan \varepsilon V_{\mathrm{dr}}}{3.44(1+3V_{\mathrm{dr}})} \\ 0 \\ \dfrac{4.06\frac{2}{\pi}\arctan \varepsilon V_{\mathrm{dr}}}{3.44(1+3V_{\mathrm{dr}})} \\ 0 \end{bmatrix}. \tag{3.15}$$

3.3.2 Path following

Path following is performed with V_{dr} as the design variable. Figs. 3.17 and 3.15 show the absolute maximum of X_1 and the free frequency of the periodic solutions, respectively. In these figures circles ($\circ$) represent stable solutions, while dots ($\cdot$) represent unstable solutions. Also, $+n$ indicates an 'in phase'

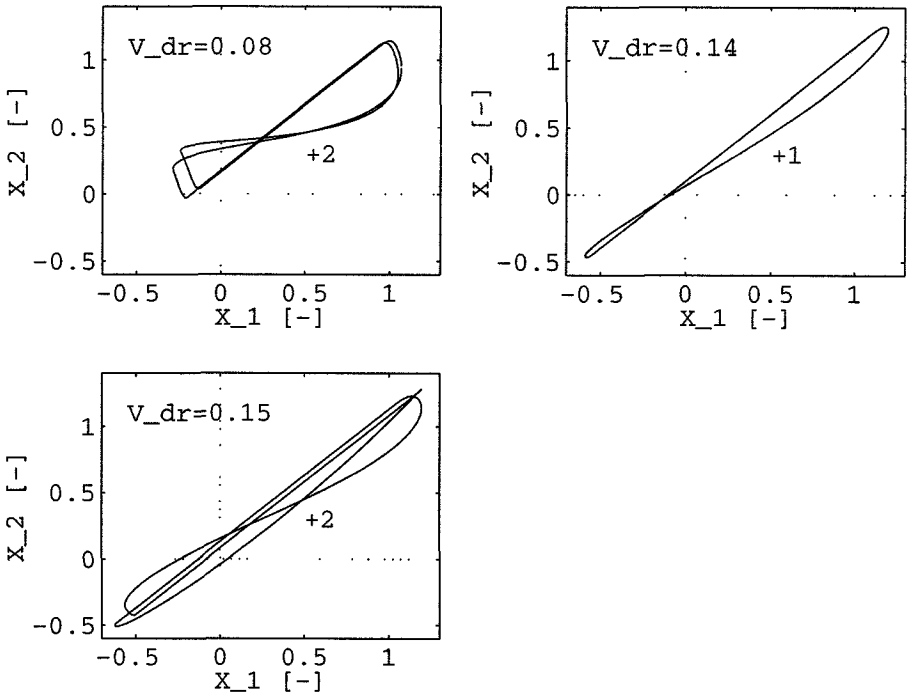

Figure 3.13: 'In phase' solutions

period-n solution branch, whereas $-n$ means 'out of phase', period-n. The boxes, containing an 'out of phase' period-8 branch and a part of -4 branch in Fig. 3.17, are enlarged in Fig. 3.16. Both for low driving belt velocities and higher period solution branches, the step size becomes very small, causing long CPU times.

The eigenfrequencies of the linear system, without dry friction, are given by $1/2\pi \approx 0.16$ and $\sqrt{1+2\alpha}/2\pi \approx 0.29$. It seems, that these frequencies are approached by the free frequencies of the unstable $+1$ and stable -1 branches, if $V_{\mathrm{dr}} \to \infty$.

Because in STRDYN, the Poincaré points of the solutions can not be determined, MATLAB is used, to make the bifurcation diagram, shown in Fig. 3.18, from the DIANA output. In this figure the Poincaré points of X_1 are plotted against V_{dr}. In the lower left part of the bifurcation diagram, the 'in phase' solution branches are located. The 'out of phase' solutions are the branches in the upper half, where the closed period-8 branch at $V_{\mathrm{dr}} \approx 0.27$ is omitted, to show the other branches more clearly. This bifurcation diagram corresponds very well to that, found by Galvanetto *et al.* [5]. However here, also branches with unstable solutions are found, along with some extra stable 'out of phase' period-4 solutions at $V_{\mathrm{dr}} \approx 0.111$, both not given in Galvanetto *et*

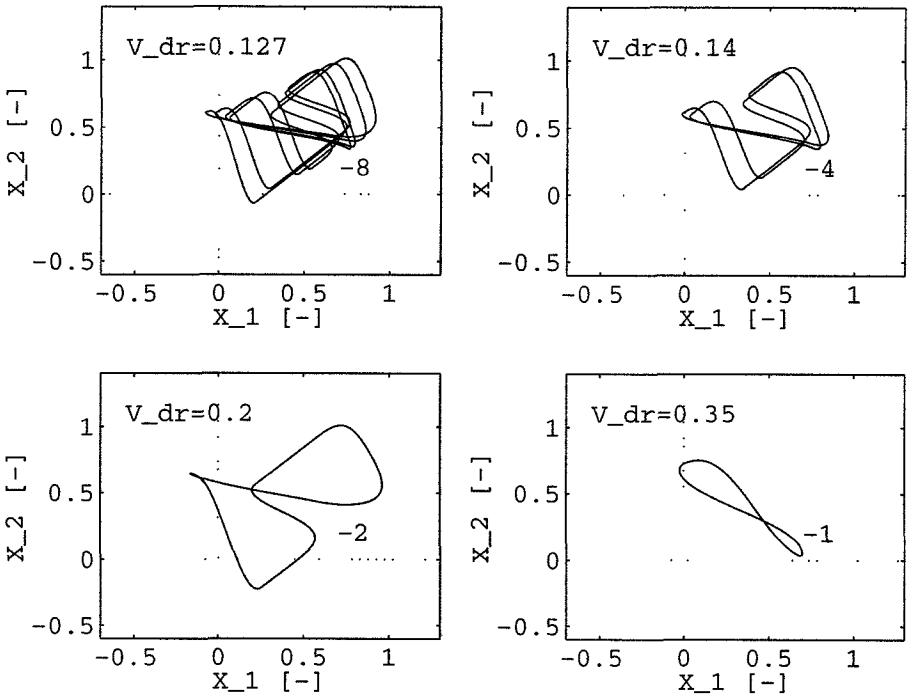

Figure 3.14: 'Out of phase' solutions

al. [5].

In Figs. 3.17 and 3.18, several types of bifurcation points can be observed. (See, for instance, Fey [4] for a description of different bifurcations.) The +1 branch shows super-critical flip bifurcations at $V_{\mathrm{dr}} = 0.081$ and 0.141. The +2 branch, leaving from 0.081, has a flip bifurcation at $V_{\mathrm{dr}} = 0.08$. The +2 branch, that is created at 0.141, undergoes a cyclic fold bifurcation at $V_{\mathrm{dr}} = 0.165$. A sub-critical flip bifurcation occurs in the −1 branch, at $V_{\mathrm{dr}} = 0.25$. The unstable −2 branch, emanating from this point becomes stable through a cyclic fold at 0.32. It changes its stability at $V_{\mathrm{dr}} = 0.29$ and 0.25, where flip bifurcations occur. At $V_{\mathrm{dr}} = 0.144$ a stable −4 branch originates from the −2 branch by a flip. This −4 branch loses its stability at 0.132 and regains it at 0.113, also by flip bifurcations. Between these bifurcation points, a stable −8 branch exists. In the −4 branch, cyclic fold bifurcations occur at $V_{\mathrm{dr}} = 0.104$ and 0.1112. Another flip bifurcation is observed in this branch, at 0.1106. In the closed −8 branch, enlarged in Fig. 3.16, cyclic folds occur at $V_{\mathrm{dr}} = 0.263$ and 0.2864 and flips are found at $V_{\mathrm{dr}} = 0.274$ and 0.2858. Between these flip bifurcations a −16 branch is found, but because of relatively large inaccuracies, due to discretization, it is not shown.

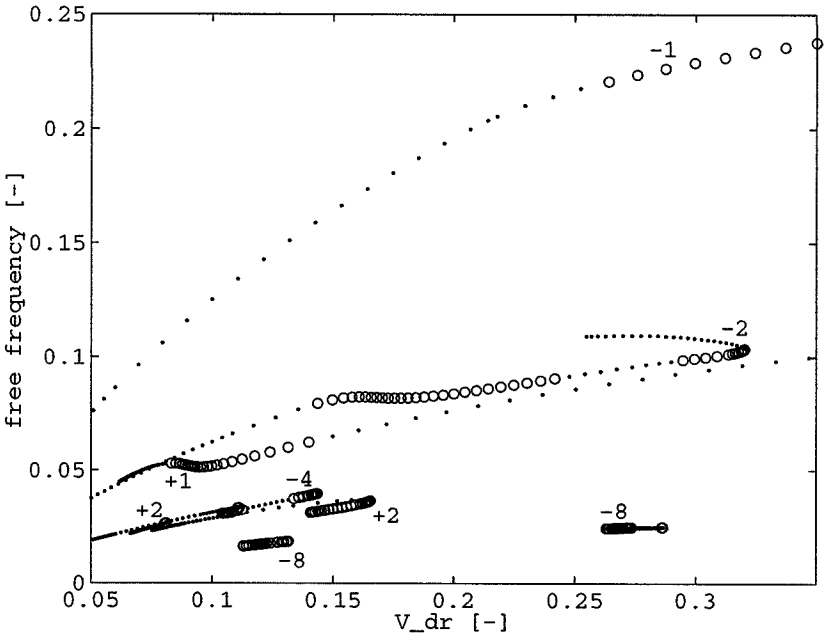

Figure 3.15: Free frequency

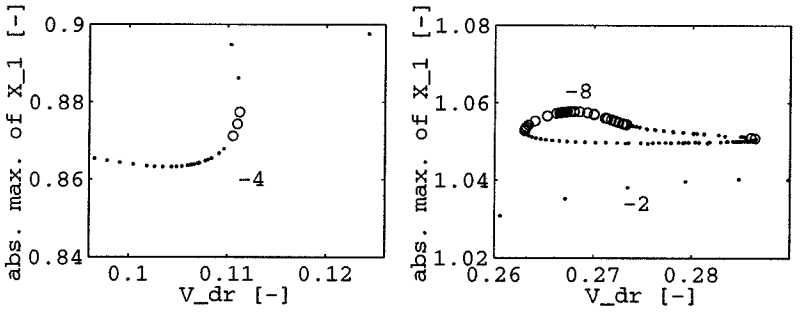

Figure 3.16: Absolute maximum of X_1

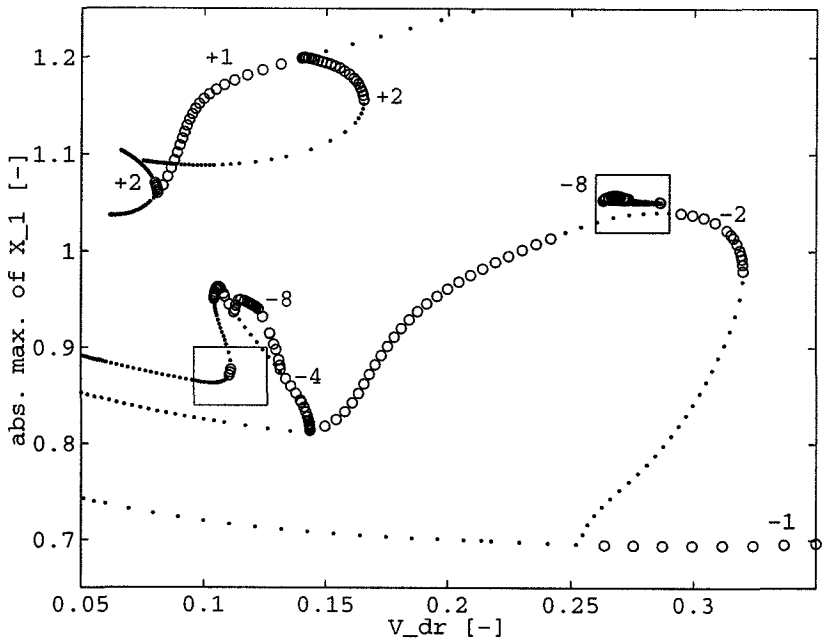

Figure 3.17: Absolute maximum of X_1

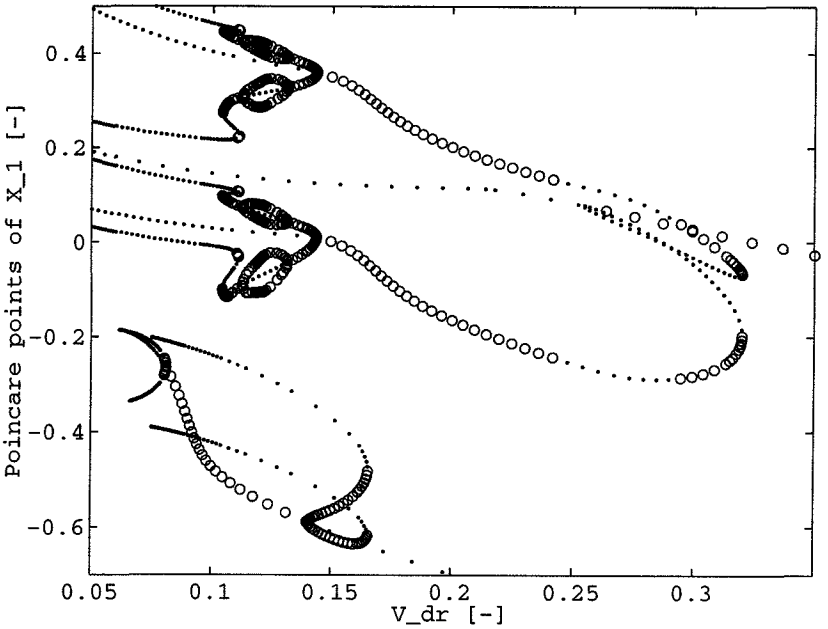

Figure 3.18: Bifurcation diagram

All calculations are repeated with $\varepsilon = 10^6$. Apart from some minor differences, this increase does not structurally change the results. The CPU times, that are used to perform the path following calculations, are given in the next table.

ε	CPU time
10^5	9 hrs. 35 min.
10^6	30 hrs. 58 min.

3.3.3 Conclusions

Apart from longer CPU times, increasing the number of DOFs of this dry friction model, does not cause problems in the DIANA calculations. The path following algorithm together with the simple shooting method works satisfactory, to find branches of periodic solutions of the approximated 2–DOF dry friction model. The results, found with DIANA, correspond very well to those, found in literature. DIANA can not make bifurcation diagrams of autonomous systems.

Chapter 4

Drill string model

In this chapter, a 1–DOF drill string model, taken from Jansen [8], is analyzed with STRDYN. In this model, Coulomb's friction law is used, which displays an even stronger discontinuity, than the friction forces, applied in the previous chapter. Again, using semi-analytic solutions, error estimates are determined of the solutions, found with DIANA.

4.1 Drill string dynamics

A drill string consists of a drill bit, drill collars and stabilizers, drill pipes and a rotary table. At the top, the rotary table is rotated by an electric motor. In Fig. 4.1(a) a schematic representation of a drill string is given. The drill bit is the tool, that crushes the rock. The stabilizers are cylindrical elements, that fit loosely in the bore hole (not shown in the figure). The drill collars are thick walled pipes, that are loaded in compression, with a typical outside diameter of 9" (0.23 [m]) and inside diameter of 3" (0.076 [m]). The drill pipes, on the other hand, are loaded in tension and are slender, with a typical outside diameter of 5" (0.13 [m]) and inside diameter of 4.3" (0.11 [m]). The rotary table is a heavy disc, with a typical mass moment of inertia of 930 [Nms^2/rad].

One of the dynamic modes of a drill string is a self-sustained torsional vibration, caused by dry friction between the drill bit, the drill collars and the stabilizers on the one hand, and the rock on the other hand. In addition to this motion, also lateral and axial vibrations occur. When the drill string is undergoing a torsional stick—slip vibration, the rotary table at the top end of the drill string is rotating at a nearly constant rate, whereas the bit speed varies between zero and a speed, much higher than the speed of the rotary table.

A model for investigating the torsional vibration is proposed by Jansen [8].

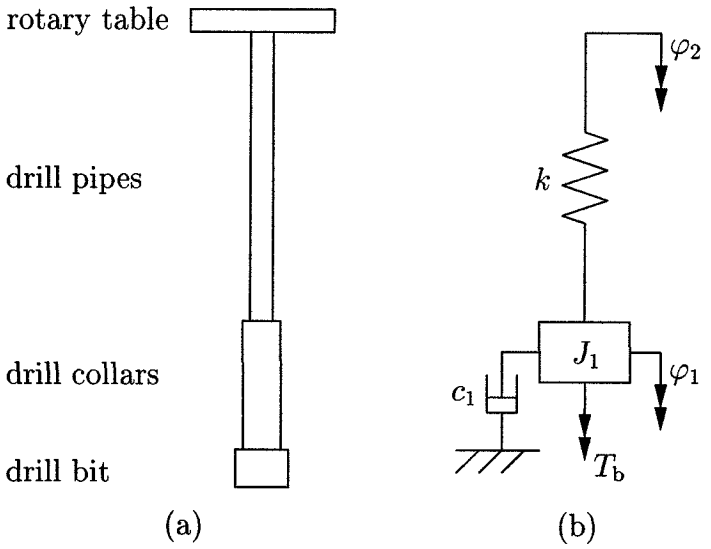

Figure 4.1: 1–DOF drill string model

In this model the drill pipes are modeled as a linear torsional spring k, as shown in Fig. 4.1(b). The drill collars are assumed to be rigid and are modeled as an equivalent mass moment of inertia J_1, also taking into account the mass moment of inertia of the drill pipes. Viscous damping is taken into account by introducing a linear torsional damper c_1. Variable φ_1 is the angular displacement of the bit and the drill collars, whereas φ_2 represents the angular displacement of the rotary table.

Dry friction is modeled by a torque T_b at the drill bit. Fig. 4.2 shows this friction torque as a function of $\dot{\varphi}_1$. This figure represents Coulomb's friction law, with a static friction torque T_{st}, that is larger than a constant dynamic friction torque T_{sl}. Here, $T_{st} = 4000$ [Nm] and $T_{sl} = 2000$ [Nm] are chosen.

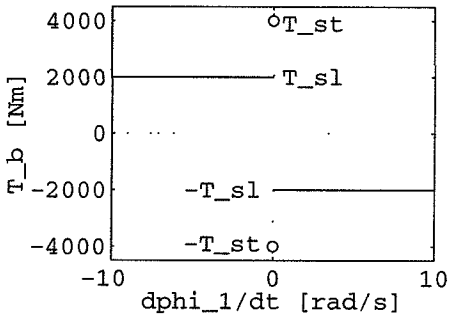

Figure 4.2: Friction torque T_b

4.2 1–DOF drill string model

4.2.1 Shooting

The 1–DOF drill string model in Fig. 4.1(b) is described by differential equation

$$J_1\ddot{\varphi}_1 + c_1\dot{\varphi}_1 + k(\varphi_1 - \varphi_2) = T_\mathrm{b}. \tag{4.1}$$

Choosing $\varphi = \varphi_2 - \varphi_1$ as the generalized coordinate and assuming, that the rotary table is rotating at a constant speed Ω_2, the equation of motion becomes

$$J_1\ddot{\varphi} + c_1\dot{\varphi} + k\varphi = -T_\mathrm{b} + c_1\Omega_2. \tag{4.2}$$

This equation possesses an equilibrium point at

$$\varphi_\mathrm{eq} = \frac{T_\mathrm{sl} + c_1\Omega_2}{k}. \tag{4.3}$$

To simplify the analysis, the following nondimensional quantities are introduced.

$$\tau = \omega t, \quad \psi = \varphi - \varphi_\mathrm{eq}, \quad \bar{\eta} = \frac{\Omega_2}{\omega}, \quad \theta = \frac{T_\mathrm{st} - T_\mathrm{sl}}{k}, \quad \zeta = \frac{c_1}{2J_1\omega}, \tag{4.4}$$

where $\omega = \sqrt{k/J_1}$ is the angular eigenfrequency of the linear system, without dry friction. With these quantities, (4.2) can be rewritten as

$$\psi'' + 2\zeta\psi' + \psi = T_\mathrm{c}, \qquad T_\mathrm{c} = -\frac{T_\mathrm{b} + T_\mathrm{sl}}{k}, \tag{4.5}$$

where a prime ($'$) denotes a differentiation to τ. The state equation is given by ($\underset{\sim}{x} = [\ \psi \quad \psi'\ ]^\mathrm{T}$)

$$\underset{\sim}{x}' = \underset{\sim}{f}(\underset{\sim}{x}) = \begin{bmatrix} \psi' \\ -2\zeta\psi' - \psi + T_\mathrm{c} \end{bmatrix}. \tag{4.6}$$

Dry friction term T_c is plotted in Fig. 4.3, as a function of ψ'. Again, a smooth approximation must be used in DIANA. It is assumed, that the drill bit does not rotate backwards and thus $\psi' \leq \bar{\eta}$. Using this, T_c is approximated by a 4th-order polynomial, given by

$$\tilde{T}_\mathrm{c} = \begin{cases} 0, & \psi' \leq q, \\ p(\psi' - \bar{\eta})(\psi' - q)^3, & \psi' > q. \end{cases} \tag{4.7}$$

Parameters p and q are found from the conditions

$$\tilde{T}_\mathrm{c}(\psi' = \bar{\eta} - \varepsilon) = \theta, \qquad \frac{\mathrm{d}\tilde{T}_\mathrm{c}}{\mathrm{d}\psi'}(\psi' = \bar{\eta} - \varepsilon) = 0, \tag{4.8}$$

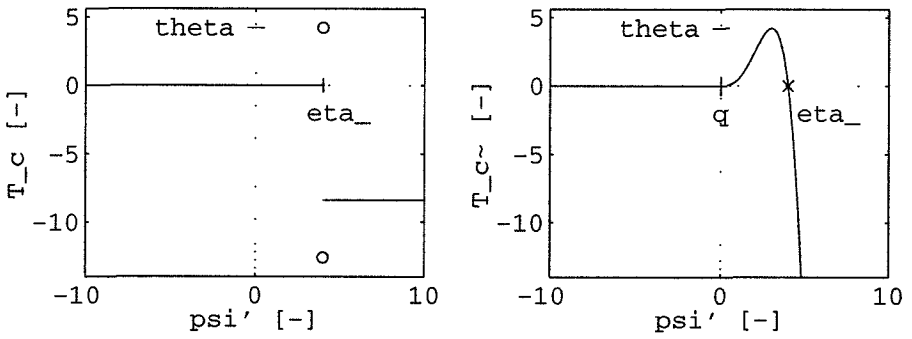

Figure 4.3: Friction term T_c and approximation $\tilde{T}_c$

and are given by

$$p = -\frac{\theta}{27\varepsilon^4}, \qquad q = \bar{\eta} - 4\varepsilon. \tag{4.9}$$

In Fig. 4.3 the approximation is plotted, for $\theta = 4.2$ and $\varepsilon = 1$. Decreasing ε will improve the approximation. Parameters ζ and θ are chosen equal to 0.05 and 4.2, respectively.

In Fig. 4.4 the stable periodic solution at $\bar{\eta} = 4$ is shown, calculated with the simple shooting method and BDF integration, for different values of ε ($\varepsilon = 10^{-i}$, $i = 0, ..., 4$). Because the original system is piecewise linear, it can be solved semi-analytically. During the stick phase, $\psi' = \bar{\eta}$, so (4.5) becomes

$$2\zeta\theta + \psi = T_c, \tag{4.10}$$

where $T_c \leq \theta$. When $\psi = \theta - 2\zeta\bar{\eta}$, the stick phase ends and the drill string starts slipping. In the slip phase, ψ and ψ' are given by

$$\psi(\tau) = e^{-\zeta\tau}\left(\psi_0 \cos\sqrt{1-\zeta^2}\tau + \frac{\psi_0' + \zeta\psi_0}{\sqrt{1-\zeta^2}} \sin\sqrt{1-\zeta^2}\tau\right), \tag{4.11}$$

$$\psi'(\tau) = e^{-\zeta\tau}\left(\psi_0' \cos\sqrt{1-\zeta^2}\tau - \frac{\psi_0 + \zeta\psi_0'}{\sqrt{1-\zeta^2}} \sin\sqrt{1-\zeta^2}\tau\right), \tag{4.12}$$

where $\psi_0 = \theta - 2\zeta\bar{\eta}$ and $\psi_0' = \bar{\eta}$. The slip phase ends, when $\psi' = \bar{\eta}$. This point can be found with the Newton–Raphson algorithm (this makes the solution *semi*-analytic). The circles (o) in Fig. 4.4 represent the semi-analytic solution, determined with MATLAB. This solution corresponds to the limit cycles, given in Jansen [8].

Errors e_ψ in the absolute maximum of ψ and e_f in the free frequency are defined as in (3.7) and (3.8), where x is exchanged with ψ. In Fig. 4.5, the errors at $\bar{\eta} = 4$ are plotted with circles (o), using double logarithmic scales. The dashed lines in this figure are least squares fits with function $e(\varepsilon) = b\varepsilon^a$, where a and b are given in the next table.

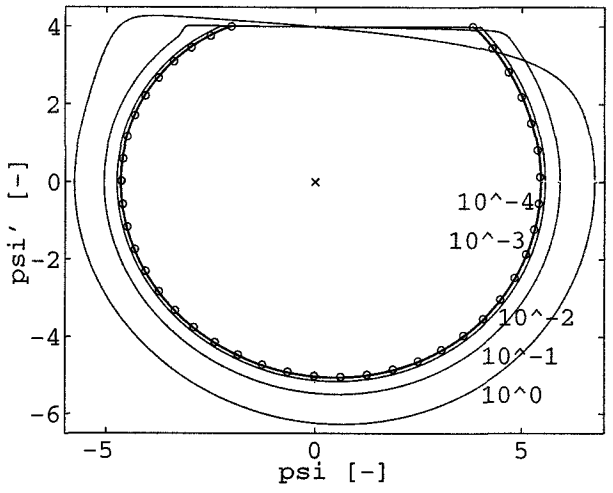

Figure 4.4: Periodic solutions at $\bar{\eta} = 4$

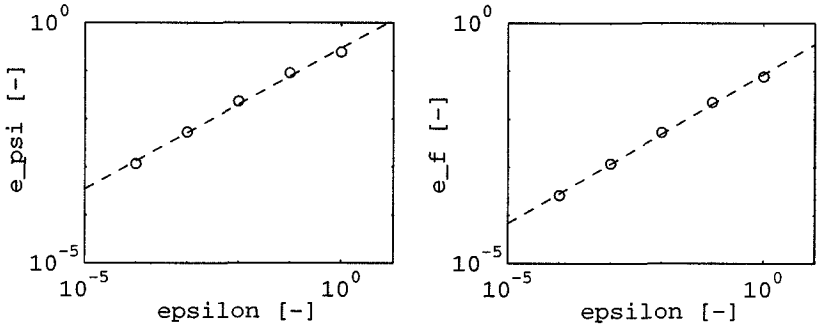

Figure 4.5: Errors e_ψ and e_f for $\bar{\eta} = 4$

	e_ψ	e_f
a	0.59	0.62
b	−0.53	−1.1

This system possesses a stable equilibrium point, given by $\underset{\sim}{x}_{\text{eq}} = [\ 0 \quad 0\ ]^{\text{T}}$. In Fig. 4.4 this equilibrium point is represented by the x–mark (×). If, however, approximation $\tilde{T}_{\text{c}}$ is used, the equilibrium point is located at $\tilde{\underset{\sim}{x}}_{\text{eq}} = [\ \tilde{\psi}_{\text{eq}} \quad 0\ ]^{\text{T}}$, where

$$\tilde{\psi}_{\text{eq}} = \begin{cases} -\dfrac{\theta}{27\varepsilon^4}\bar{\eta}(\bar{\eta} - 4\varepsilon)^3, & \bar{\eta} < 4\varepsilon, \\ 0, & \bar{\eta} \geq 4\varepsilon. \end{cases} \tag{4.13}$$

When $\bar{\eta}$ is decreased below some value $\bar{\eta}_{\text{bif},1} = \bar{\eta}_{\text{bif},1}(\varepsilon)$, this equilibrium point becomes unstable (if $\zeta < 8\theta/27\varepsilon$). At $\bar{\eta}_{\text{bif},2} = \bar{\eta}_{\text{bif},2}(\varepsilon)$ it becomes stable again.

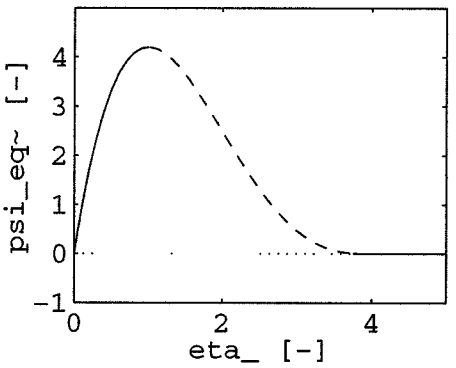

Figure 4.6: Equilibrium point $\tilde{\psi}_{\text{eq}}$ ($\varepsilon = 1$)

This does not correspond to the original system, where the equilibrium point is always stable. Fig. 4.6 shows $\tilde{\psi}_{\text{eq}}$ as a function of $\bar{\eta}$, for $\varepsilon = 1$, where $\bar{\eta}_{\text{bif},1} \approx 3.759$ and $\bar{\eta}_{\text{bif},2} \approx 1.018$. The solid lines represent stable equilibrium points, the dashed line unstable ones.

4.2.2 Path following

Parameter $\bar{\eta}$ is used as the design variable in path following. Again, the calculations are repeated for different values of ε ($\varepsilon = 10^{-i}$, $i = 0, ..., 4$). Figs. 4.7 and 4.8 show the absolute maximum of ψ and the free frequency of the periodic solutions. All branches are stable. Here, $\bar{\eta}$ is subsequently decreased from 4 towards 0 and increased from 4. About 6 minutes of CPU time are needed per branch.

If $\bar{\eta} \downarrow 0$, the absolute maximum of ψ should approach $\theta - 2\zeta\bar{\eta} = 4.2$, the point at which the stick phase ends. The free frequency should approach 0, because of a longer stick phase at low values of $\bar{\eta}$. If $\bar{\eta}$ is increased, at some point, the limit cycle should disappear. Because of damping, $\psi'(\tau)$ from (4.12) does not become equal to $\bar{\eta}$ anymore and the stable equilibrium point is reached. Smaller values of ε show a better correspondence to these conditions.

MATLAB is used, to calculate semi-analytic solutions at $\bar{\eta} = 1$, 2 and 3, and parameters a and b of the relative errors are determined. In Fig. 4.9, these parameters are shown as functions of $\bar{\eta}$. The solid lines belong to error e_ψ, the dashed lines to e_f. Again, a is approximately constant and b increases, if $\bar{\eta}$ is decreased. The parameters are also given in the next table.

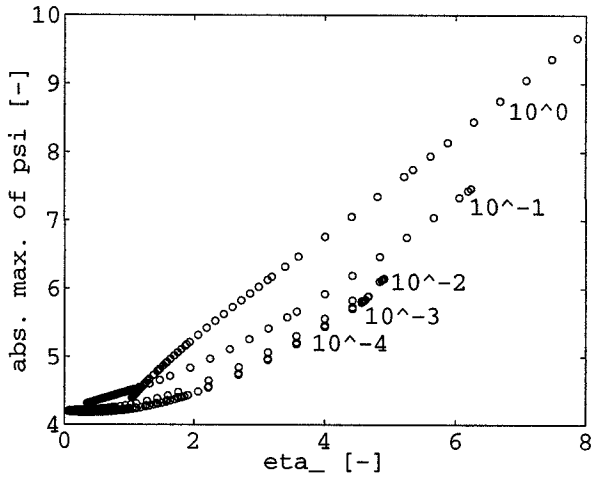

Figure 4.7: Absolute maximum of ψ

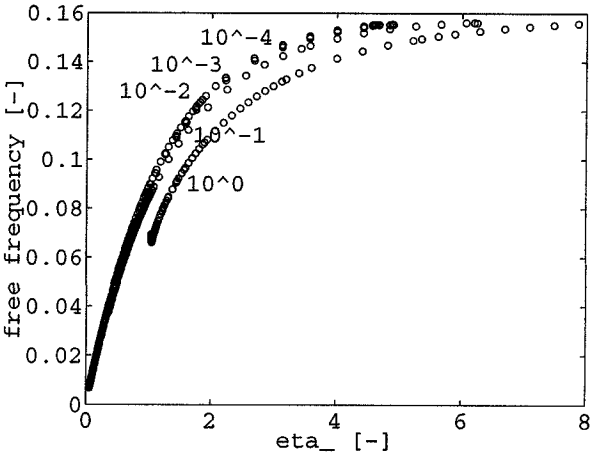

Figure 4.8: Free frequency

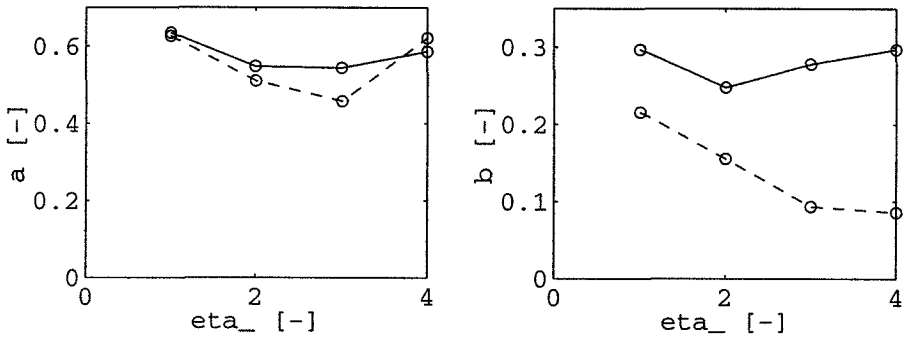

Figure 4.9: Parameters a and b

	$\bar{\eta}$	1	2	3	4
e_ψ	a	0.63	0.55	0.54	0.59
	b	0.30	0.25	0.28	0.30
e_f	a	0.63	0.51	0.46	0.62
	b	0.22	0.16	0.093	0.086

4.2.3 Conclusions

The 1–DOF drill string model can successfully be analyzed with DIANA, when the friction torque is approximated, using a 4th-order polynomial. The results, found with STRDYN, correspond to what is found by Jansen [8].

Chapter 5

Conclusions

- Using a smooth approximation and applying BDF integration, both dry friction with a decreasing dynamic friction coefficient for increasing absolute relative velocity and Coulomb's friction law can successfully be modeled in DIANA. Applying simple shooting and the path following algorithm, periodic solutions can be found with module STRDYN.
- Module STRDYN, exhibits some limitations in analyzing autonomous systems. Due to numerical errors, the stability of periodic solutions is not determined correctly. A bifurcation diagram can not be made from the calculated solution branches, because Poincaré points can not be determined. Also, STRDYN lacks an algorithm for finding equilibrium points.
- Good correspondence is found between results of DIANA calculations and those, found in literature.

Appendix A

The variational equation

An nth-order, autonomous, nonlinear dynamic system is represented by the state equation with initial condition[1]

$$\dot{\underset{\sim}{x}} = \underset{\sim}{f}(\underset{\sim}{x}), \qquad \underset{\sim}{x}(t=0) = \underset{\sim}{x}_0. \tag{A.1}$$

The solution to this equation is written as $\underset{\sim}{\phi}_t(\underset{\sim}{x}_0)$, so

$$\dot{\underset{\sim}{\phi}}_t(\underset{\sim}{x}_0) = \underset{\sim}{f}(\underset{\sim}{\phi}_t(\underset{\sim}{x}_0)), \qquad \underset{\sim}{\phi}_0(\underset{\sim}{x}_0) = \underset{\sim}{x}_0. \tag{A.2}$$

Differentiating with respect to $\underset{\sim}{x}_0$ gives

$$\frac{\partial \dot{\underset{\sim}{\phi}}_t(\underset{\sim}{x}_0)}{\partial \underset{\sim}{x}_0} = \frac{\partial \underset{\sim}{f}}{\partial \underset{\sim}{x}} \frac{\partial \underset{\sim}{\phi}_t(\underset{\sim}{x}_0)}{\partial \underset{\sim}{x}_0}, \qquad \frac{\partial \underset{\sim}{\phi}_0(\underset{\sim}{x}_0)}{\partial \underset{\sim}{x}_0} = \underline{I}. \tag{A.3}$$

Defining $\underline{\Phi}_t(\underset{\sim}{x}_0) \equiv \partial \underset{\sim}{\phi}_t(\underset{\sim}{x}_0)/\partial \underset{\sim}{x}_0$, (A.3) becomes

$$\dot{\underline{\Phi}}_t(\underset{\sim}{x}_0) = \frac{\partial \underset{\sim}{f}}{\partial \underset{\sim}{x}} \underline{\Phi}_t(\underset{\sim}{x}_0), \qquad \underline{\Phi}_0(\underset{\sim}{x}_0) = \underline{I}, \tag{A.4}$$

which is the *variational equation.*

Since the initial condition is the identity matrix, $\underline{\Phi}_t(\underset{\sim}{x}_0)$ is the fundamental matrix of the set of linear differential equations (A.4). It follows, that a perturbation $\delta \underset{\sim}{x}_0$ of $\underset{\sim}{x}_0$ evolves as

$$\delta \underset{\sim}{x}(t) = \underline{\Phi}_t(\underset{\sim}{x}_0) \delta \underset{\sim}{x}_0. \tag{A.5}$$

[1]The derivation, presented in this appendix, is taken from Parker and Chua [10].

Appendix B

User subroutines

B.1 1–DOF dry friction model (ndsptr.f)

```
C...
C...   d_2: v_dr
C...   d_3: eps
C...
C...   force = 2/pi*atan(eps*v_rel)/(1+3*abs(v_rel))
C...   v_rel = tvelta-v_dr
C...
      SPSTIF = 0.D0
      VREL = TVELTA-DESVL(2)
      EPS = DESVL(3)
C
      TFORCE = 2.D0/PI*ATAN(EPS*VREL)/(1.D0+3.D0*ABS(VREL))
      SPDAMP = 2.D0/PI*EPS/(1.D0+(EPS*VREL)**2)/(1.D0+3.D0*ABS(VREL))-
     $         6.D0/PI*ATAN(EPS*VREL)*SIGN(1.D0,VREL)/
     $         (1.D0+3.D0*ABS(VREL))**2
C
```

B.2 2–DOF dry friction model (ndsptr.f)

```
C...
C...   d_2: beta
C...   d_3: gamma
C...   d_4: V_dr
C...   d_5: eps
C...
C...   force = 2/pi*atn(eps*V_rel)/(1+gamma*abs(V_rel))
C...   V_rel = tvelta-V_dr
C...
C...   if ELMNR=6, force = beta*force
C...
      SPSTIF = 0.D0
      BETA = DESVL(2)
      GAMMA = DESVL(3)
      VREL = TVELTA-DESVL(4)
      EPS = DESVL(5)
C
      TFORCE = 2.D0/PI*ATAN(EPS*VREL)/(1.D0+GAMMA*ABS(VREL))
```

```
      SPDAMP = 2.D0/PI*EPS/(1.D0+(EPS*VREL)**2)/(1.D0+GAMMA*ABS(VREL))-
     $         GAMMA*2.D0/PI*ATAN(EPS*VREL)*SIGN(1.D0,VREL)/
     $         (1.D0+GAMMA*ABS(VREL))**2
C
      IF ( ELMNR .EQ. 6 ) THEN
         TFORCE = BETA*TFORCE
         SPDAMP = BETA*SPDAMP
      ENDIF
C
```

B.3 1–DOF drill string model (`ndspro.f`)

```
C...
C...   d_1: f_free
C...   d_2: eta_
C...   d_3: theta
C...   d_4: zeta
C...   d_5: eps
C...
C...   force = 2*zeta*tvelta - T_c
C...
C...     | T_c
C...     |
C...     - theta          ..
C...     |              .  .
C...     |             ..   .
C...     |          ...      .
C...     |      ....         .
C...    ..+.....+----------+---+-----------
C...     0|   eta_      eta_  eta_     tvelta
C...      |  -4*eps     -eps    .
C...
C...  -T_c = 0                                    if tvelta <= eta_-4*eps
C...         theta*(tvelta-eta_)*(tvelta-eta_+4*eps)^3/(27*eps^4)    else
C...
      ETA = DESVL(2)
      THETA = DESVL(3)
      ZETA = DESVL(4)
      EPS = DESVL(5)
      TFORCE = 2.D0*ZETA*TVELTA
      SPSTIF = 0.D0
      SPDAMP = 2.D0*ZETA
      IF ( TVELTA .GT. ETA-4.D0*EPS ) THEN
         TFORCE = TFORCE + THETA*(TVELTA-ETA)*(TVELTA-ETA+4.D0*EPS)**3/
     $            (27.D0*EPS**4)
         SPDAMP = SPDAMP + 4.D0*THETA*(TVELTA-ETA+EPS)*
     $            (TVELTA-ETA+4.D0*EPS)**2/(27.D0*EPS**4)
      END IF
C
```

Bibliography

[1] D. H. van Campen and A. de Kraker. *Het Dynamisch Gedrag van Constructies.* Syllabus, Eindhoven University of Technology, Eindhoven, The Netherlands, 1990/1991. (In Dutch.)

[2] D. H. van Campen. *Niet-lineaire Dynamica.* Syllabus, Eindhoven University of Technology, Eindhoven, The Netherlands, 1991. (In Dutch.)

[3] DIANA *User's Manual, release 6.0.* TNO Building and Construction Research, Delft, The Netherlands, 1995.

[4] R. H. B. Fey, *Steady-state Behaviour of Reduced Dynamic Systems with Local Nonlinearities.* Ph.D. thesis, Eindhoven University of Technology, Eindhoven, The Netherlands, 1992.

[5] U. Galvanetto, S. R. Bishop and L. Briseghella. Mechanical Stick—Slip Vibrations, *International Journal of Bifurcation and Chaos,* Vol. 5, No. 3, pp. 637–651. World Scientific Publishing Company, 1995.

[6] M. Hénon. On the Numerical Computation of Poincaré Map, *Physica D* 5, pp. 412–414. 1982.

[7] A. C. Hindmarsh. ODEPACK, A Systematized Collection of ODE Solvers, *Scientific Computing,* Vol 1, R. Stepleman *et al.* (eds.), pp. 55–64. IMACS/North-Holland Publishing Company, Amsterdam, 1983.

[8] J. D. Jansen, *Nonlinear Dynamics of Oilwell Drillstrings.* Ph.D. thesis, Delft University Press, Delft, The Netherlands, 1993.

[9] M. Oestreich, N. Hinrichs, K. Popp. Bifurcation and Stability Analysis for a Non-Smooth Friction Oscillator, *Archive of Applied Mechanics* 66, pp. 301–314. Springer-Verlag, 1996.

[10] T. S. Parker and L. O. Chua. *Practical Numerical Algorithms for Chaotic Systems.* Springer-Verlag, New York, 1989.

[11] K. Popp and P. Stelter. Nonlinear Oscillations of Structures Induced by Dry Friction, *Nonlinear Dynamics in Engineering Systems,* IUTAM Symposium Stuttgart/Germany 1989, pp. 233–240. Springer-Verlag, Berlin Heidelberg, 1990.

[12] E. L. B. van de Vorst, *Long Term Dynamics and Stabilization of Nonlinear Mechanical Systems.* Ph.D. thesis, Eindhoven University of Technology, Eindhoven, The Netherlands, 1996.